*nutrients*

MDPI

*Article*

# Untargeted Metabolomics and Chemometrics Elucidate Dynamic Plasma Profile Changes Induced by Cocoa Shell in Female Rats

**David Ramiro-Cortijo [1,2,†], Miguel Rebollo-Hernanz [2,3,4,†], Pilar Rodríguez-Rodríguez [1,2], Santiago Ruvira [1,2], Silvia M. Arribas [1,2,*] and Maria A. Martin-Cabrejas [2,3,4,*]**

[1] Department of Physiology, Faculty of Medicine, Universidad Autónoma de Madrid, C/Arzobispo Morcillo 2, 28029 Madrid, Spain; david.ramiro@uam.es (D.R.-C.); pilar.rodriguezr@uam.es (P.R.-R.); santiago.ruvira@estudiante.uam.es (S.R.)
[2] Food, Oxidative Stress and Cardiovascular Health (FOSCH) Research Group, Universidad Autónoma de Madrid, 28049 Madrid, Spain; miguel.rebollo@uam.es
[3] Department of Agricultural Chemistry and Food Science, Faculty of Science, Universidad Autónoma de Madrid, C/Francisco Tomás y Valiente, 7, 28049 Madrid, Spain
[4] Institute of Food Science Research (CIAL, UAM-CSIC), Universidad Autónoma de Madrid, C/Nicolás Cabrera, 9, 28049 Madrid, Spain
* Correspondence: silvia.arribas@uam.es (S.M.A.); maria.martin@uam.es (M.A.M.-C.)
† Both authors contributed equally and should be considered as first authors.

**Abstract:** Objective: This study aimed to explore the effects of cocoa shell extract (CSE) supplementation on the plasma metabolome of female rats. Methods: Female rats were supplemented with CSE (250 mg/kg/day) over seven days, and plasma samples were collected at baseline, day 4, and day 7 for untargeted metabolomic profiling using LC-ESI-QTOF. Results: A total of 244 plasma metabolites were identified, while 180 were detected in the CSE. Among these, only 21 compounds were consistently detected in both the CSE and the plasma at baseline and day 7. Notably, just three compounds, caffeine, theobromine, and *N*-isovaleroylglycine, were bioavailable, detected only in plasma after supplementation on day 7, confirming their absorption and systemic distribution. Pathways related to caffeine metabolism, glycerophospholipid biosynthesis, nicotinate, and nicotinamide metabolism were significantly upregulated, indicating enhanced lipid metabolism and energy homeostasis. Conversely, reductions were observed in pathways involving tryptophan, glutathione, arginine, and proline, pointing to shifts in amino acid metabolism and antioxidant defense mechanisms. Network analysis revealed significant changes in the cholinergic synapse, retrograde endocannabinoid signaling, and glutamatergic synapse pathways, which are crucial for cellular communication and neurotransmission. Conclusions: The observed metabolic reconfiguration demonstrates CSE's rapid modulation of the metabolome, highlighting the bioavailability of its key components. These findings suggest potential mechanisms for CSE as a functional food ingredient with health-promoting effects, potentially supporting cognitive function and metabolic health through energy metabolism, neurotransmission, and lipid signaling pathways.

**Keywords:** cocoa shell extract; metabolomics; bioavailability; methylxanthines; lipid metabolism; energy homeostasis; neurotransmission; functional food; cocoa by-product



Academic Editor: Edgard Delvin

Received: 17 January 2025
Revised: 19 February 2025
Accepted: 27 February 2025
Published: 28 February 2025

**Citation:** Ramiro-Cortijo, D.; Rebollo-Hernanz, M.; Rodríguez-Rodríguez, P.; Ruvira, S.; Arribas, S.M.; Martin-Cabrejas, M.A. Untargeted Metabolomics and Chemometrics Elucidate Dynamic Plasma Profile Changes Induced by Cocoa Shell in Female Rats. *Nutrients* **2025**, *17*, 885. https://doi.org/10.3390/nu17050885



## 1. Introduction

The expanding field of nutraceuticals shows an increasing interest in potential applications of food industry by-products [1]. As efforts to minimize waste and optimize resources are gaining attention, these frequently underutilized by-products are becoming recognized

for their significant health-promoting properties. They represent a vast and largely unexplored resource, and up-cycling them into value-added products, such as bioactive food ingredients and nutraceuticals, not only supports sustainable development goals, but can also contribute to reducing the burden of chronic diseases [2]. Cocoa shell is an excellent example of an underutilized by-product generated during chocolate processing, usually discarded in large quantities. Recently, cocoa shell has been uncovered as a safe bioactive food ingredient, due to its rich nutritional composition and the absence of potential toxic effects [3]. Despite its classification as waste, cocoa shell is rich in bioactive compounds, such as methylxanthines, (poly)phenols, and dietary fiber, among others, which have been linked to a variety of health benefits, including antioxidant, anti-inflammatory, lipid-lowering, and vasoactive properties [4,5]. The presence of these beneficial compounds in cocoa shell has attracted considerable interest in exploring its potential role in health promotion, as it has potential in preventing diseases [6,7], particularly those associated with metabolic and cardiovascular dysregulation [8]. These diseases represent a significant global health burden, due to their high prevalence and associated mortality rates. Consequently, dietary interventions, especially those involving natural compounds, emerge as promising strategies for these health issues [9]. In this context, cocoa shell appears as a promising alternative, with the added value of representing an important milestone in the sustainable use of food by-products for health promotion.

Whereas the bioaccessibility, related colonic microbiota biotransformation, and potential absorption of methylxanthines and (poly)phenols from cocoa shell have been investigated in vitro [10], a comprehensive understanding of its bioavailability and subsequent impact on the metabolome remains unexplored. Metabolomics is a powerful tool for investigating this gap, as it allows for a comprehensive analysis of the small-molecule metabolites present in a biological system [11] and complex biochemical responses to dietary interventions, providing insights into their mechanistic foundation [12]. Untargeted metabolomics allows for a broad-spectrum view of the metabolome, identifying changes in the levels of multiple metabolites simultaneously, regardless of prior assumptions. This approach can lead to a better knowledge of the systemic effects of dietary intake, which is essential for developing effective bioactive food ingredients and nutraceuticals, advancing our comprehension of nutrition's role in health and disease [13]. In addition, chemometric techniques can complement metabolomic analyses, and identify patterns and relationships among the complex array of plasma metabolites using advanced statistical methods, thereby highlighting the primary compounds and pathways affected by dietary interventions [14]. These observations may provide insights into the probable mechanisms through which cocoa shell exerts its beneficial effects.

Considering the limited data on the metabolic effects of cocoa shell extract, the present study aims to investigate the impact of CSE intake on the rat plasma metabolome. By employing untargeted metabolomics and chemometric analysis, we seek to identify the key metabolites and enrichment metabolic pathways influenced by cocoa shell, thereby elucidating the plasmatic changes induced by this dietary intervention. Our results could provide novel insights into the mechanisms implicated in the health-promoting properties of cocoa shell, potentially guiding its utilization as a bioactive food ingredient or nutraceutical.

## 2. Materials and Methods

### *2.1. Preparation of Cocoa Shell Extract*

The cocoa (*Theobroma cacao*) shell used in this study, supplied by Chocolates Santocildes (Castrocontrigo, León, Spain), was of the high-quality "Criollo Carenero" variety from Barlovento (Barlovento, Venezuela), processed with long fermentation and low-temperature oak wood drum roasting. CSE was prepared using an optimized extraction protocol [15].

First, the cocoa shell was milled, and then the ground cocoa shell was combined with boiling water (20 g/L). The mixture was stirred continuously for 90 min, and the CSE was filtered and frozen at −20 °C for 24 h. The extract was then freeze-dried and stored at −20 °C until further use.

### 2.2. Formulation of Cocoa Shell Supplement

The CSE supplement was prepared using gelatin as a vehicle, as previously described [16]. Briefly, the gelatin cubes were formulated using 100% bovine gelatin (Inkafoods, S.L., Barcelona, Spain) dissolved in water (140 g/L). To produce the cubes, water was heated to a temperature of 50–60 °C, and the gelatin was gradually added, while stirring continuously, until it completely dissolved. At this stage, various additives were introduced into the mixture, including vanilla flavor (4.8 mL/L; MyProtein, Hut.com Ltd., Manchester, UK) and sucralose (0.6 g/L sucralin, Sucralose S.L., Barcelona, Spain) as non-caloric flavoring agent and sweetener, respectively. Two types of gelatin cubes were produced: (i) neutral cubes without CSE (vehicle) and (ii) CSE-enriched gelatins (treatment). In this case, the CSE was incorporated into the mixture after the gelatin had dissolved. The gelatin mixture was then carefully poured into a mold, ensuring even distribution, to form cubes with a size of 1 $cm^3$. The dose of CSE used in the study was 250 mg/kg/day, which was calculated based on the rat's weight and the cube's size. A comprehensive flow chart of the experimental design is depicted inFigure 1.

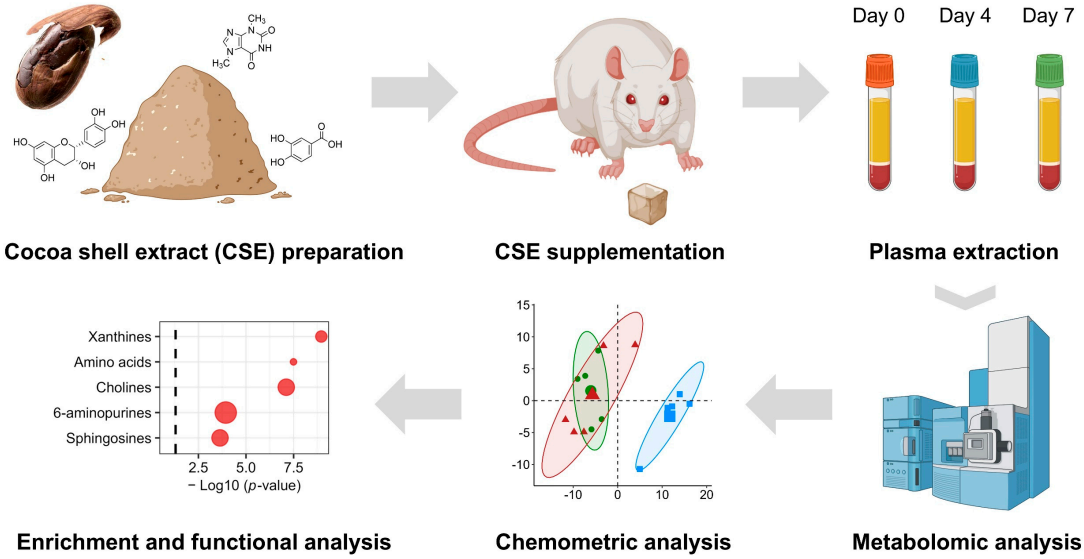


**Figure 1.** A flow chart of the experimental design. This diagram outlines the steps involved in the experimental procedure for CSE supplementation analysis. Starting with the preparation of the cocoa shell extract (CSE), the chart depicts the subsequent phases, including the administration of CSE to the female rats, the collection of biological samples at defined time points, and the metabolomic analysis. The latter involves mass spectrometry-based metabolite identification, data processing, and subsequent bioinformatics and chemometric analysis, including pathway- and network-based enrichment analyses.

### 2.3. Protocol for Cocoa Shell Supplementation in Female Rats

Five-month-old adult female Sprague Dawley rats from the breeding colony at the animal house facility of Universidad Autónoma de Madrid (ES-28079-0000097) were utilized for the study. The experimental procedures adhered to the Guidelines for the Care and Use of Laboratory Animals (National Institutes of Health publication no. 85–23, revised in 1996), Spanish legislation (RD 53/2013), and the Directive 2010/63/EU on the protection of animals. Ethical approval was obtained from the Ethics Review Board of Universidad

Autónoma de Madrid and the Regional Committee of Comunidad Autónoma de Madrid (PROEX 19/04; approval date: 20 March 2019). The rats were group-housed in type III cages (24 cm × 19 cm × 45 cm; length × height × width) with poplar bedding, accommodating 3–5 rats per cage. Environmental enrichment was provided using cellulose nestles and play tunnels (Index Research S.L., Madrid, Spain). The animals were maintained under controlled temperature (22 °C), humidity (40%), and a 12 h light–dark cycle. They were fed ad libitum with a diet containing 51.7% carbohydrates, 21.4% protein, 5.1% lipids, 3.9% fiber, 5.7% minerals, and 12.2% humidity (SafeA03; Safe-Lab, Augy, France). Drinking water was also available ad libitum. Training staff regularly monitored animal health to ensure that the rats were free from any pathogens that could influence the study parameters.

CSE supplementation was performed through voluntary ingestion. The rats were first trained to accept the new food using neutral gelatin cubes for 3–5 days, following a previously established protocol [16]. After the training phase, the rats were supplemented with CSE-enriched gelatin cubes for a period of 7 days. Blood samples were collected from the rats on day 0 (baseline, non-supplemented), day 4, and day 7. The blood samples were collected in restrained rats through the tail vein, using tubes preloaded with 5% heparin. The blood was centrifuged at 900× *g* for 10 min at 4 °C, and the plasma was aliquoted and stored at −80 °C for further analysis. The rats were not sacrificed as part of this specific study. However, they were used in a subsequent study, after which they were humanely euthanized with $CO_2$ exposure, followed by exsanguination [16].

### *2.4. Sample Preparation for Untargeted Metabolomic Analysis*

#### 2.4.1. Preparation of CSE

CSE was weighed (10 mg) and added to a 2 mL tube. Then, 1 mL of MeOH:$H_2O$ (80:20 *v*/*v*) was added to the tube. The tube was placed in a Thermomixer and agitated at 2000 rpm, for 2 min, at a temperature of 4 °C. Subsequently, the tube was subjected to cold sonication for 10 min. After sonication, the tube was centrifuged at 12,000× *g*, for 10 min, at a low temperature, and the supernatant was collected without disturbing any solid particles settled at the bottom of the vial. This supernatant was then suitable for injection. A blank extraction sample was also prepared, following the same extraction protocol used for the experimental samples to ensure accuracy and control for potential interferences.

#### 2.4.2. Preparation of Plasma Samples

Samples were thawed on ice and homogenized using a vortex for 30 s. Then, 200 µL of plasma was mixed with 800 µL of MeOH, previously cooled to −20 °C. The mixture was vortexed for 2 min and incubated at −20 °C for 1 h. Subsequently, the samples were centrifuged at 12,000× *g* for 15 min at 4 °C. The supernatant (600 µL) was collected without disturbing the solid particles at the bottom of the vial. The supernatant was dried using a Speed-vac for 5 h at room temperature. For reconstitution, 200 µL of MeOH:$H_2O$ (80:20 *v*/*v*) was added, followed by vortexing for 2 min and 30 s. The reconstituted solution was centrifuged at 12,000× *g* for 10 min at 4 °C, and the supernatant was collected, without disturbing any solid particles at the bottom of the vial, for injection. A blank extraction sample was prepared, following the same extraction protocol as the experimental samples.

### *2.5. Untargeted Metabolomic Analysis by LC-ESI-QTOF*

An Agilent 1290 Infinity UHPLC system (Santa Clara, CA, USA) was used for metabolomic analysis, equipped with a binary pump, a diode array detector, and a Peltier-cooled autoinjector. This system combined ultra-high pressures (up to 1200 bar) with high mobile-phase flow rates (up to 5 mL/min). The exact mass spectrometer used was the Agilent 6540 UHD (Santa Clara, CA, USA), with a quadrupole time-of-flight (Q/TOF) analyzer and an ESI Jet Stream interface (Santa Clara, CA, USA). The column used was a Zorbax

Eclipse Plus C18 (1.8 µm, 2.1 × 100 mm), coupled with a Zorbax C18 precolumn (1.8 µm, 2.1 × 5 mm) from Agilent (Santa Clara, CA, USA). The column temperature was maintained at 40 °C, and the injection volume was set to 2 µL. The mobile phase consisted of phase A (0.1% formic acid in $H_2O$) and phase B (0.1% formic acid in acetonitrile), with a 0.5 mL/min flow rate. The gradient started with 0% of the organic mobile phase B (0.1% formic acid in acetonitrile) at the beginning of the analysis, and it increased linearly to 100% over 13 min. At 14 min, the gradient rapidly changed to 0% organic mobile phase, and this composition was maintained for 3 min for column equilibration before the next injection. Detection was performed using TOF-MS in positive mode, with a mass range of 25–1100 $m/z$ and a scan rate of 5 spectra/s. The ionization source was AJS-ESI, and the gas temperature was 300 °C. The drying gas flow rate was 8 L/min, the nebulizer pressure was 40 Psi, and the sheath gas temperature was 350 °C, with a flow rate of 11 L/min. The capillary voltage was set at 3000 V, and the fragmentor and skimmer voltages were 110 V and 45 V, respectively. Reference masses for calibration were $m/z$ 121.050873 (purine) and 922.009798 (HP-0921). The same TOF conditions were applied for Q-TOF MS/MS analysis in the positive mode. Collision energies (CID) of 20 and 40 were used for fragmentation studies. The samples were injected randomly to eliminate any drift effects that could arise from the instrument or analysis conditions. Blank injections were intercalated after each sample injection to monitor the proper elution of sample components, prevent sample contamination (carry-over), and improve reproducibility. Three replicates were performed for each sample and blank extraction, with a blank injection ($H_2O$ MilliQ) between each replicate.

### *2.6. Data Statistical Analysis*

#### 2.6.1. Data Curation and Processing

The chromatograms acquired were processed using MS-DIAL software (version 4.6) (http://prime.psc.riken.jp/compms/msdial/main.html (accessed on 19 September 2024)). All the sample and extraction blank files (.d) were converted to .abf format and simultaneously analyzed. Peak detection was performed using the retention time and the exact mass, and the MS2Dec deconvolution algorithm was utilized. This algorithm initially extracts the MS/MS spectra for each precursor peak across all chromatograms, then employs least squares optimization to extract the "model peaks". Finally, the pure MS/MS spectrum is determined by the maximum heights of the reconstructed chromatograms. Peak alignment was subsequently carried out, and compound identification was performed using the exact mass, isotope ratio, and MS/MS spectrum similarity, by comparison with various databases (NIST20, MoNA, and LipidBlast).

For post-processing of the data, the median of the heights of each triplicate injection was considered. A series of filtering steps were then conducted. This involved eliminating all peaks whose maximum height in the samples was less than three times the average height of the peak in the extraction blanks. Furthermore, all peaks with a maximum height in the samples of less than 1000 intensity units were excluded. In addition, all peaks not identified as metabolites in the matched libraries were discarded, along with any peaks not quantified in at least three samples from any group. According to the PubChem repository (https://pubchem.ncbi.nlm.nih.gov/), each peak was identified with the InChIKey code. Subsequently, the low limit of detection (LLD) was considered as the lowest level of intensity in the identified metabolite. To avoid artifacts in the statistical analysis, the non-detected intensity of metabolite was filled with ½ of LLD. Finally, duplicates were eliminated, and the adducts and fragments found for the same metabolite were grouped using the bioinformatics tool MS-FLO (https://msflo.fiehnlab.ucdavis.edu/). This comprehensive data curation process ensured the accuracy and reliability of the subsequent metabolomic analysis.

2.6.2. Univariate Statistical Analysis

The metabolomic analysis followed the workflow described in Chen et al. [17]. The analysis was performed by R software version 4.4.1 (R Core Team 2022. R Foundation for Statistical Computing, Vienna, Austria; https://www.R-project.org/ (accessed on 3 July 2024) with the RStudio interface (version 2023.06.0+421 for Windows; Boston, MA, USA). Overall, the packages used were *rio*, *dplyr*, *compareGroups*, *ggplot2*, *ggpubr*, *grid*, and *gridExtra*; the specified packages are described below. A *p*-value of less than 0.05 was considered statistically significant in all analyses. The distribution of each metabolite was examined using the Shapiro–Wilk test, to ensure that the subsequent analysis was applicable. The metabolite variables were logarithmically converted and reported as medians and interquartile ranges.

The categorical variables were summarized as relative frequencies. Univariate analysis was used to identify differences in the abundance of the metabolites over time. Considering the same individual, a repeated Mann–Whitney test was performed when day 4 was excluded. In addition, the *p*-value was adjusted for multiple comparisons by false discovery rate (FDR).

2.6.3. Multivariate Chemometric Analysis

This analysis was performed using Principal Component Analysis (PCA), subclass fold change, and heat maps of metabolites by time points. This analysis was carried out by the *omu* [18], *pheatmap*, *FactoMineR* [19], and *factoextra* packages. Firstly, the metabolomic data were normalized by typification and scaled between −1 and 1. This step was essential to ensure that all variables were on a comparable scale, avoiding undue influence from variables with large numeric ranges. Secondly, unsupervised PCA was carried out to capture the maximum variance in the dataset, by reducing its dimensionality while preserving the essential similarities and differences between the samples. The analysis was performed simultaneously on all samples for the three replicates, to identify patterns and visualize clustering. The PCA was performed following the sphericity assumption based on Barlett´s test. To avoid overlapping in the metabolomic variables, the standardized loading was extracted from the varimax-rotated matrix, and each sample's weight in the first and second principal components (PCs) was reported.

In addition, heatmap and dendrogram analyses were performed to classify the samples by time. This visual approach allows an intuitive understanding of the relationships among the samples based on their metabolic profiles, highlighting the distinct clusters within the data, and, thus, corroborating the findings from the PCA and fold change analysis. The metabolomic data were classified according to Euclidian distance and clustered by the Ward method. For an appropriate interpretation, the metabolic variables were split according to significant differences in the fold change for their subclass.

2.6.4. Pathway and Enrichment Analysis

The InChIKey codes were matched with their Human Metabolome Database (HMDB) ID, Kyoto Encyclopedia of Genes and Genomes (KEGG) ID, and PubChem Compound Identification (CID) using a chemical translation service (http://cts.fiehnlab.ucdavis.edu/ (accessed on 19 September 2024)) [20]. All metabolites had a PubChem CID, but not all metabolites were identified by the HMDB and KEGG, because metadata were unavailable for some. Then, the pathway and enrichment analyses were performed by the MetaboAnalyst 5.0 platform (https://www.metaboanalyst.ca/MetaboAnalyst/ (accessed on 19 September 2024)). The metabolites identified were contrasted with the pathways available in all libraries for the *Rattus norvegicus* model, using relative-betweenness centrality in the topology analysis and hypergeometric test. For the pathway analysis, the pathway

impact was calculated as the sum of the importance measures of the matched metabolites divided by the sum of the importance measures of all metabolites in each pathway, and the logarithmic *p*-value was extracted. In addition, for the enrichment analysis, the metabolites were clustered by subclass of chemical structure, and the enrichment ratio was computed as the observed hits introduced as metabolites divided by the expected hits of the pathway. Both the logarithmic *p*-value transformed and the FDR-adjusted *p*-value were extracted and plotted.

#### 2.6.5. Functional Analysis of Metabolic Changes

The functional analysis was conducted with a multivariate strategy to identify the major drivers of differences between time and visualize complex patterns in the metabolomic data. Then, the InChIKey codes were clustered, extracting subclasses of compounds according to the PubChem repository registered in the MeSH Three classification, LIPID MAPS Classification, or KEGG: Metabolite classification. Metabolites not found in any of the libraries were categorized as "*unknown*". The fold change at the end of the cocoa shell supplementation (day 7) was compared to the baseline (basal time). Significant fold changes in the subclasses, adjusted for FDR, were then extracted.

#### 2.6.6. Functional Enrichment Through Network-Based Analysis

To elucidate the functional implications of our metabolomic data, we utilized the FELLA (Functional Enrichment analysis using Latent variable models for Metabolomics data) package in R [21]. The analysis aimed to integrate metabolomic data with KEGG pathway information to identify enriched pathways and key metabolites. The input for this analysis comprised significantly modified metabolites, with significant fold changes adjusted for FDR, compared to the baseline. The KEGG data were loaded from a preconstructed local database encompassing pathway, enzyme, reaction, compound, and module information. Identified metabolites were mapped onto the KEGG graph to perform the functional enrichment analysis, prioritizing metabolites and pathways based on their relevance in the metabolic network. The diffusion method was applied with a set number of 100 iterations to ensure robust results. The results were visualized by generating a network graph using FELLA. The top-scoring nodes were determined based on a stringent *nlimit* parameter set to 150, and enriched pathways were exported for further analysis. This approach allowed for the effective integration and interpretation of metabolomic data within the context of established metabolic pathways, highlighting critical areas for subsequent investigation.

## 3. Results

### *3.1. Comprehensive Analysis of CSE Showed Key Metabolic Pathways and Chemical Structures*

The comprehensive metabolomic analysis of the CSE identified a total of 180 compounds, highlighting the complexity of the extract's chemical profile (Table 1). Detailed data on retention times, molecular formulae, ion adducts, and mass-to-charge ratios ($m/z$) with associated errors in parts per million (ppm) underline the robustness of the analysis. To better contextualize these findings, we have provided an expanded supplementary table (Supplementary Table S1) listing the major compounds identified, their putative metabolic pathways, and their potential health effects. Given the untargeted nature of this metabolomic study, absolute quantification is not available. However, semi-quantitative abundance counts allow for relative comparisons among metabolites. The analysis revealed a wide array of phytochemicals and bioactive compounds, reflecting the diverse chemical nature of the CSE. After adjusting for FDR, the predominant chemical structures identified were several key classes of compounds, particularly amino acids and

xanthines. Among the amino acids, phenylalanine ($[M+H]^+$ = 166.08574 $m/z$) and betaine ($[M+H]^+$ = 118.08614 $m/z$) were highly represented, reflecting their significant roles in protein synthesis and methylation processes.

**Table 1.** Comprehensive metabolomic profile of cocoa shell extract (CSE), showing identified metabolites, their chemical families, retention times ($R_t$), molecular formulas, adducts, and mass-to-charge ratios ($m/z$), along with observed errors and relative abundances.

| Metabolite Name | Chemical Family | $R_t$ (min) | Formula | Adduct | Observed *m/z* | Calculated *m/z* | Error (ppm) | Cocoa Shell (Count × $10^4$) |
|---|---|---|---|---|---|---|---|---|
| Caffeine | Xanthines | 3.073 | $C_8H_{10}N_4O_2$ | $[M+H]^+$ | 195.08735 | 195.08771 | −1.8 | 181.8716 |
| Nicotinoylglycine | Amino acids | 2.392 | $C_8H_8N_2O_3$ | $[2M+H]^+$ | 181.06001 | 181.06050 | −2.7 | 176.9846 |
| Choline cation | Cholines | 0.569 | $C_5H_{14}NO$ | $[Cat]^+$ | 104.10646 | 104.10700 | −5.2 | 109.5438 |
| Betaine | Amino acids | 0.589 | $C_5H_{12}NO_2{}^+$ | $[M+H]^+$ | 118.08614 | 118.08570 | 3.7 | 68.2777 |
| Phenylalanine | Amino acids | 3.870 | $C_9H_{11}NO_2$ | $[M+H]^+$ | 166.08574 | 166.08600 | −1.6 | 62.9024 |
| L-Isoleucine | Amino acids | 1.323 | $C_6H_{13}NO_2$ | $[M+H]^+$ | 132.10197 | 132.10190 | 0.5 | 59.1781 |
| DL-Norvaline | Amino acids | 0.648 | $C_5H_{11}NO_2$ | $[M+H]^+$ | 118.08676 | 118.08677 | −0.1 | 49.8276 |
| (3-nitrophenyl)methanol | Benzyl alcohols | 2.983 | $C_7H_7NO_3$ | $[M+H]^+$ | 154.05022 | 154.04990 | 2.1 | 28.7702 |
| *N*-(2-Pyridylmethyl)piperazine-1-ethylamine | Piperazines | 0.589 | $C_{12}H_{20}N_4$ | $[M+H]^+$ | 221.17647 | 221.17610 | 1.7 | 28.0571 |
| DL-Norleucine | Amino acids | 2.209 | $C_6H_{13}NO_2$ | $[M+H]^+$ | 132.10193 | 132.10193 | 0.0 | 21.5649 |
| 2-Hydroxyphenethylamine | Phenethylamine | 2.773 | $C_8H_{11}NO$ | $[M+H]^+$ | 120.08086 | 120.08080 | 0.5 | 18.2369 |
| *N*-Acetyl-L-glutamic acid | Amino acids | 1.148 | $C_7H_{11}NO_5$ | $[M+H]^+$ | 172.06044 | 172.06039 | 0.3 | 18.2252 |
| 3,4-Cyclopropylglutamate | Amino acids | 1.043 | $C_6H_9NO_4$ | $[M+H]^+$ | 140.03476 | 140.03529 | −3.8 | 15.7238 |
| Asperglaucide | Dipeptides | 7.996 | $C_{27}H_{28}N_2O_4$ | $[M+Na]^+$ | 467.19397 | 467.19400 | −0.1 | 12.9412 |
| Stachydrine | Pyrrolidine alkaloids | 0.708 | $C_7H_{13}NO_2$ | $[M+H]^+$ | 144.10246 | 144.10190 | 3.9 | 11.8364 |
| Tris(2,4-di-tert-butylphenyl)phosphate | Organophosphorus compounds | 13.926 | $C_{42}H_{63}O_4P$ | $[M+H]^+$ | 663.45374 | 663.45367 | 0.1 | 10.8888 |
| 5-oxo-D-Proline | Amino acids | 0.990 | $C_5H_7NO_3$ | $[M+H]^+$ | 130.04996 | 130.04997 | −0.1 | 10.7441 |
| 7-Methylxanthine | Xanthines | 2.075 | $C_6H_6N_4O_2$ | $[M+H]^+$ | 167.05612 | 167.05635 | −1.4 | 10.5532 |
| L-Proline | Amino acids | 7.990 | $C_5H_9NO_2$ | $[M+H]^+$ | 117.06997 | 117.07000 | −0.3 | 9.5794 |
| 1-Aminocyclohexanecarboxylic acid | Amino acids | 1.814 | $C_7H_{13}NO_2$ | $[M+H]^+$ | 144.10184 | 144.10190 | −0.4 | 9.0652 |
| Val-Val | Dipeptides | 2.529 | $C_{10}H_{20}N_2O_3$ | $[M+H]^+$ | 217.15448 | 217.15469 | −1.0 | 8.2541 |
| Ugandenial A | Sesquiterpenes | 1.911 | $C_{15}H_{22}O_4$ | $[M+H]^+$ | 289.13965 | 289.14102 | −4.7 | 8.1922 |
| L-Tyrosine | Amino acids | 3.966 | $C_9H_{11}NO_3$ | $[M+H]^+$ | 182.08141 | 182.08141 | 0.0 | 7.7061 |
| Koninginin E | Benzopyrans | 1.262 | $C_{16}H_{26}O_5$ | $[M+H]^+$ | 321.16577 | 321.16571 | 0.2 | 7.3375 |
| D-Pipecolinic acid | Carboxylic acid | 3.121 | $C_6H_{11}NO_2$ | $[M+H]^+$ | 259.16425 | 259.16519 | −3.6 | 6.0300 |
| Leu-Val | Dipeptides | 2.622 | $C_{11}H_{22}N_2O_3$ | $[M+H]^+$ | 231.17027 | 231.17030 | −0.1 | 6.0071 |
| 5-phenyllevulinic acid | Carboxylic acids | 2.864 | $C_{11}H_{12}O_3$ | $[M+K]^+$ | 210.11296 | 210.11301 | −0.2 | 5.8234 |
| Leu-Ile | Dipeptides | 3.068 | $C_{12}H_{24}N_2O_3$ | $[M+H]^+$ | 245.18800 | 245.18600 | 8.2 | 5.7594 |
| (Z)-5,8,11-trihydroxyoctadec-9-enoic acid | Fatty acids | 6.224 | $C_{18}H_{34}O_5$ | $[M+NH_4]^+$ | 348.27463 | 348.27341 | 3.5 | 5.5588 |
| Piperidine | Piperidines | 1.310 | $C_5H_{11}N$ | $[M+H]^+$ | 86.09669 | 86.09694 | −2.9 | 5.5261 |
| Pro-Val | Dipeptides | 2.062 | $C_{10}H_{18}N_2O_3$ | $[M+H]^+$ | 215.13892 | 215.13901 | −0.4 | 5.4371 |
| *N*-Acetylproline | Amino acids | 2.238 | $C_7H_{11}NO_3$ | $[2M+K]^+$ | 158.08084 | 158.08119 | −2.2 | 5.4242 |
| 1-Palmitoyl-2-oleoylphosphatidylserine | Phospholipids | 12.570 | $C_{40}H_{76}NO_{10}P$ | $[M+Na]^+$ | 780.55267 | 780.55249 | 0.2 | 5.2930 |
| L-Pipecolic acid | Piperidines | 2.308 | $C_6H_{11}NO_2$ | $[M+H]^+$ | 112.07574 | 112.07570 | 0.4 | 5.1864 |
| 6-Hydroxynicotinic acid | Pyridine carboxylic acids | 1.169 | $C_6H_5NO_3$ | $[M+H]^+$ | 140.03412 | 140.03419 | −0.5 | 5.1694 |
| 5-Hydroxy-2-(hydroxymethyl)pyridine | Piridines | 0.749 | $C_6H_7NO_2$ | $[M+H]^+$ | 126.05507 | 126.05500 | 0.6 | 5.0079 |
| *trans*-2-dodecenedioic acid | Fatty acids | 3.313 | $C_{12}H_{20}O_4$ | $[M+Na]^+$ | 251.12547 | 251.12540 | 0.3 | 4.7774 |
| 4-Guanidinobutyric acid | Guanidines | 2.388 | $C_5H_{11}N_3O_2$ | $[M+NH_4]^+$ | 434.24939 | 434.24811 | 2.9 | 4.5778 |
| Nicotinic acid | Pyridine carboxylic acids | 0.897 | $C_6H_5NO_2$ | $[M+H]^+$ | 124.03944 | 124.03943 | 0.1 | 4.4967 |
| Ile-Phe | Dipeptides | 3.424 | $C_{15}H_{22}N_2O_3$ | $[M+H]^+$ | 279.17035 | 279.17029 | 0.2 | 4.3652 |
| L-Tryptophan | Amino acids | 2.567 | $C_{11}H_{12}N_2O_2$ | $[M+H]^+$ | 205.09715 | 205.09715 | 0.0 | 4.3597 |
| Ser-Tyr-Lys | Tripeptides | 2.187 | $C_{18}H_{28}N_4O_6$ | $[M+NH_4]^+$ | 199.10767 | 199.10770 | −0.2 | 4.2192 |
| PE 17:0/22:6 | Phospholipids | 12.401 | $C_{44}H_{75}O_8P$ | $[M+H]^+$ | 780.55450 | 780.55383 | 0.9 | 4.1227 |
| Procyanidin B2 | (Poly)phenols | 2.794 | $C_{30}H_{26}O_{12}$ | $[M+H]^+$ | 579.14984 | 579.14972 | 0.2 | 4.0849 |
| (+)-Catechin | (Poly)phenols | 3.273 | $C_{15}H_{14}O_6$ | $[M+H]^+$ | 291.08630 | 291.08630 | 0.0 | 4.0531 |
| Aurantiamide | Dipeptides | 7.012 | $C_{25}H_{26}N_2O_3$ | $[M+H]^+$ | 403.20200 | 403.20111 | 2.2 | 4.0333 |
| 1,3,7-Trimethyluric acid | Xanthines | 2.754 | $C_8H_{10}N_4O_3$ | $[M+H]^+$ | 211.08286 | 211.08299 | −0.6 | 3.7675 |
| 4-Methylquinolin-2-ol | Quinolines | 0.539 | $C_{10}H_9NO$ | $[M+K]^+$ | 319.14383 | 319.14410 | −0.8 | 3.7625 |
| Gentiobiose | Disaccharide | 0.595 | $C_{12}H_{22}O_{11}$ | $[M+K]^+$ | 381.07919 | 381.07938 | −0.5 | 3.7047 |
| MGDG O-9:0/22:6 | Galactolipids | 13.582 | $C_{40}H_{66}O_9$ | $[M+H]^+$ | 708.50733 | 708.50452 | 4.0 | 3.7007 |
| Phenylethylamine | Phenylethylamines | 2.311 | $C_8H_{11}N$ | $[M+H-NH_3]^+$ | 105.06991 | 105.06990 | 0.1 | 3.6676 |
| 2-Aminophenol | Aminophenols | 0.961 | $C_6H_7NO$ | $[M+H]^+$ | 110.06028 | 110.06020 | 0.7 | 3.6554 |
| MGDG 2:0/6:0 | Galactolipids | 4.118 | $C_{17}H_{30}O_{10}$ | $[M+NH_4]^+$ | 412.21765 | 412.21771 | −0.1 | 3.6006 |
| Pyrrole-2-carboxylic acid | Pyrrole carboxylic acids | 2.984 | $C_5H_5NO_2$ | $[M+H]^+$ | 112.03905 | 112.03930 | −2.2 | 3.5997 |
| Dianthoside | Triterpenes | 3.004 | $C_{12}H_{16}O_8$ | $[2M+Na]^+$ | 289.09192 | 289.09201 | −0.3 | 3.5732 |
| L-Leucine | Amino acids | 1.956 | $C_6H_{13}NO_2$ | $[M+H]^+$ | 132.10172 | 132.10172 | 0.0 | 3.5372 |
| Trigonelline | Alkaloids | 0.611 | $C_7H_7NO_2$ | $[M+H]^+$ | 138.05518 | 138.05495 | 1.7 | 3.5338 |
| 3,7-Dihydroxyflavone | (Poly)phenols | 2.421 | $C_{15}H_{10}O_4$ | $[2M+H]^+$ | 255.1194 | 255.11984 | −1.7 | 3.4200 |
| cAMP | Ribonucleotides | 1.967 | $[C_{10}H_{11}N_5O_6P]^-$ | $[M+Na]^+$ | 268.10422 | 268.10410 | 0.4 | 3.3707 |
| Ferulamide | (Poly)phenols | 3.196 | $C_{10}H_{11}NO_3$ | $[M+H]^+$ | 194.08067 | 194.08099 | −1.6 | 3.3350 |
| Pro-Ile | Dipeptides | 1.132 | $C_{11}H_{20}N_2O_3$ | $[M+H]^+$ | 229.15486 | 229.15469 | 0.7 | 3.3262 |
| PC 8:0/30:7 | Phospholipids | 11.867 | $C_{46}H_{78}NO_8P$ | $[M+Na]^+$ | 804.55298 | 804.55377 | −1.0 | 3.3210 |
| Pantothenic acid | Carboxylic acids | 2.273 | $C_9H_{17}NO_5$ | $[M+H]^+$ | 220.11768 | 220.11760 | 0.4 | 3.2063 |
| 1,2-Dipalmitoyl-sn-glycero-3-phospho-(1′-rac-glycerol) | Phospholipids | 13.668 | $C_{38}H_{75}O_{10}P$ | $[M+H]^+$ | 721.50586 | 721.50250 | 4.7 | 3.1628 |
| 5-Aminovaleric acid | Amino acids | 2.134 | $C_5H_{11}NO_2$ | $[M+H]^+$ | 100.07556 | 100.07570 | −1.4 | 3.1572 |
| MGDG O-8:0/12:0 | Galactolipids | 9.514 | $C_{29}H_{56}O_9$ | $[M+H]^+$ | 566.42761 | 566.42627 | 2.4 | 3.0768 |
| Val-Phe | Dipeptides | 2.987 | $C_{14}H_{20}N_2O_3$ | $[M+H]^+$ | 265.15451 | 265.15469 | −0.7 | 2.9783 |

**Table 1.** *Cont.*

| Metabolite Name | Chemical Family | $R_t$ (min) | Formula | Adduct | Observed *m/z* | Calculated *m/z* | Error (ppm) | Cocoa Shell (Count × $10^4$) |
|---|---|---|---|---|---|---|---|---|
| Theobromine | Xanthines | 2.589 | $C_7H_8N_4O_2$ | $[M+H]^+$ | 181.07198 | 181.07201 | −0.2 | 2.9773 |
| 4-Acetamidobutanoic acid | Amino fatty acids | 1.912 | $C_6H_{11}NO_3$ | $[M+H]^+$ | 146.0809 | 146.08118 | −1.9 | 2.9351 |
| 3-Hydroxy-2-methylpyridine | Pyridine alkaloids | 0.738 | $C_6H_7NO$ | $[M+H]^+$ | 110.06017 | 110.06000 | 1.5 | 2.8867 |
| 1,2-Diamino-2-methylpropane | Alkylamines | 2.667 | $C_4H_{12}N_2$ | $[M+H]^+$ | 72.08076 | 72.08080 | −0.6 | 2.8804 |
| 2,6-Dihydroxypyridine | Pyridine alkaloids | 1.010 | $C_5H_5NO_2$ | $[M+H]^+$ | 112.03943 | 112.03933 | 0.9 | 2.8761 |
| 4-Hydroxyquinoline | Quinolines | 2.731 | $C_9H_7NO$ | $[M+H]^+$ | 146.06039 | 146.06090 | −3.5 | 2.8048 |
| Citric acid | TCA acid | 0.965 | $C_6H_8O_7$ | $[M+H]^+$ | 193.03419 | 193.03430 | −0.6 | 2.7578 |
| Glu-Ile-Arg | Tripeptides | 2.436 | $C_{17}H_{30}N_6O_5$ | $[2M+H]^+$ | 399.23471 | 399.23499 | −0.7 | 2.7442 |
| 2-Aminobenzoic acid | Carboxylic acids | 2.843 | $C_7H_7NO_2$ | $[M+H]^+$ | 138.05518 | 138.05499 | 1.4 | 2.7030 |
| Guanosine | Purine Nucleosides | 1.999 | $C_{10}H_{13}N_5O_5$ | $[M+K]^+$ | 284.09915 | 284.09906 | 0.3 | 2.6956 |
| 4-Hydroxyphenethylamine | Phenethylamines | 1.425 | $C_8H_{11}NO$ | $[M+H]^+$ | 138.09138 | 138.09129 | 0.7 | 2.6598 |
| (−)-Epicatechin | (Poly)phenols | 2.632 | $C_{15}H_{14}O_6$ | $[M+H]^+$ | 291.08655 | 291.08633 | 0.8 | 2.6549 |
| 3,4,5-Trihydroxyphenethylamine | Phenethylamines | 1.006 | $C_8H_{11}NO_3$ | $[M+H]^+$ | 168.06577 | 168.06660 | −4.9 | 2.6351 |
| Sorbicillin | Phenols | 1.522 | $C_{14}H_{16}O_3$ | $[M+H]^+$ | 231.10338 | 231.10271 | 2.9 | 2.6254 |
| Ala-Ile | Dipeptides | 2.237 | $C_9H_{18}N_2O_3$ | $[M+H]^+$ | 203.1384 | 203.13850 | −0.5 | 2.5838 |
| 3-Hydroxypicolinic acid | Pyridines | 2.983 | $C_6H_5NO_3$ | $[M+H]^+$ | 122.02402 | 122.02370 | 2.6 | 2.5708 |
| 2-(2-Ethylbutanoylamino)-4,5-dimethoxybenzoic acid | Carboxylic acids | 3.164 | $C_{15}H_{21}NO_5$ | $[M+H]^+$ | 250.14453 | 250.14490 | −1.5 | 2.5577 |
| *p*-Carboxymethylphenylalanine | Amino acids | 2.215 | $C_{11}H_{13}NO_4$ | $[M+H]^+$ | 224.09134 | 224.09171 | −1.7 | 2.4812 |
| (9Z,12E)-15,16-dihydroxyoctadeca-9,12-dienoic acid | Fatty acids | 6.950 | $C_{18}H_{32}O_4$ | $[M+H]^+$ | 313.2373 | 313.23734 | −0.1 | 2.4777 |
| *N*-Isovaleroylglycine | Amino acids | 0.738 | $C_7H_{13}NO_3$ | $[M+H]^+$ | 160.09671 | 160.09680 | −0.6 | 2.4453 |
| (+)-Cathinone | Alkaloids | 4.316 | $C_9H_{11}NO$ | $[M+H]^+$ | 299.17529 | 299.17542 | −0.4 | 2.4319 |
| *N*-Acetyl-β-D-mannosamine | Amino sugar | 1.101 | $C_8H_{15}NO_6$ | $[M+H-C_2H_8O_4]^+$ | 126.05508 | 126.05500 | 0.6 | 2.4197 |
| 4-Aminophenol | Aminophenols | 2.388 | $C_6H_7NO$ | $[M+H]^+$ | 110.05943 | 110.05890 | 4.8 | 2.4185 |
| Kynurenic acid | Xanthurenates | 2.824 | $C_{10}H_7NO_3$ | $[M+H]^+$ | 190.04955 | 190.04950 | 0.3 | 2.3696 |
| Pro-Trp | Dipeptides | 3.067 | $C_{16}H_{19}N_3O_3$ | $[M+H]^+$ | 302.15033 | 302.14990 | 1.4 | 2.3584 |
| Anabasamine | Alkaloids | 2.069 | $C_{16}H_{19}N_3$ | $[M+Na]^+$ | 254.16515 | 254.16518 | −0.1 | 2.3187 |
| MGDG 2:0/3:0 | Galactolipids | 2.606 | $C_{14}H_{24}O_{10}$ | $[M+NH_4]^+$ | 370.17099 | 370.17078 | 0.6 | 2.3122 |
| Harmine | Alkaloids | 2.428 | $C_{13}H_{12}N_2O$ | $[M+H]^+$ | 213.11624 | 213.11636 | −0.6 | 2.1951 |
| *N*-*cis*-*p*-Coumaroyltyrosine | (Poly)phenols | 4.062 | $C_{18}H_{17}NO_5$ | $[M+H]^+$ | 328.11798 | 328.11795 | 0.1 | 2.1564 |
| Guanine | Purine | 2.000 | $C_5H_5N_5O$ | $[M+Na]^+$ | 152.05716 | 152.05721 | −0.3 | 2.1498 |
| SM (34:1;O2) | Phospholipids | 13.742 | $C_{37}H_{63}N_2O_6P$ | $[M+H]^+$ | 685.43457 | 685.43158 | 4.4 | 2.1476 |
| Kavain | Pyrans | 1.231 | $C_{14}H_{14}O_3$ | $[M+H]^+$ | 231.10153 | 231.10156 | −0.1 | 2.0343 |
| Jaeschkeanadiol | Sesquiterpenes | 8.098 | $C_{15}H_{26}O_2$ | $[M+H]^+$ | 256.22699 | 256.22708 | −0.4 | 1.9400 |
| 4,6-Dioxoheptanoic acid | Fatty acids | 2.754 | $C_7H_{10}O_4$ | $[M+H]^+$ | 141.05466 | 141.05460 | 0.4 | 1.9085 |
| Sclareol | Diterpenoids | 11.403 | $C_{20}H_{36}O_2$ | $[M+H]^+$ | 326.3049 | 326.30533 | −1.3 | 1.8766 |
| Cyclo(Leu-Pro) | Dipeptides | 3.570 | $C_{11}H_{18}N_2O_2$ | $[M+H]^+$ | 211.14395 | 211.14391 | 0.2 | 1.8738 |
| Tyr-Gly-Gly-Phe-Leu | Peptides | 7.012 | $C_{28}H_{37}N_5O_7$ | $[M+Na]^+$ | 425.18323 | 425.18188 | 3.2 | 1.8470 |
| Methacholine | Cholines | 0.852 | $C_8H_{18}NO_2$ | $[M+H]^+$ | 160.13336 | 160.13319 | 1.1 | 1.8445 |
| Hypoxanthine | Xanthines | 1.030 | $C_5H_4N_4O$ | $[M+H]^+$ | 137.04565 | 137.04570 | −0.4 | 1.8251 |
| Val-Tyr | Dipeptides | 2.287 | $C_{14}H_{20}N_2O_4$ | $[M+H]^+$ | 281.14932 | 281.14960 | −1.0 | 1.8210 |
| Leu-Gly | Dipeptides | 1.991 | $C_8H_{16}N_2O_3$ | $[M+H]^+$ | 189.12323 | 189.12340 | −0.9 | 1.8165 |
| *N*-Carboxyethyl-γ-aminobutyric acid | Amino acids | 0.807 | $C_7H_{13}NO_4$ | $[M+H]^+$ | 176.09164 | 176.09171 | −0.4 | 1.8102 |
| 9-Oxo-10E,12Z-octadecadienoic acid | Fatty acids | 6.239 | $C_{18}H_{30}O_3$ | $[M+H]^+$ | 295.22675 | 295.22681 | −0.2 | 1.8013 |
| Oxazole-4-carboxylic acid | Carboxyl acids | 0.472 | $C_4H_3NO_3$ | $[M+H]^+$ | 112.00468 | 112.00400 | 6.1 | 1.8009 |
| L-Saccharopine | Amino acids | 0.985 | $C_{11}H_{20}N_2O_6$ | $[M+H]^+$ | 275.12485 | 275.12491 | −0.2 | 1.7431 |
| Phe-Gly | Dipeptides | 2.294 | $C_{11}H_{14}N_2O_3$ | $[M+NH_4]^+$ | 223.10759 | 223.10770 | −0.5 | 1.7342 |
| L-Carnitine | Amino acids | 0.603 | $C_7H_{15}NO_3$ | $[M+H]^+$ | 162.11243 | 162.11000 | 15.0 | 1.6820 |
| Ala-Val | Dipeptides | 0.950 | $C_8H_{16}N_2O_3$ | $[M+H]^+$ | 189.12366 | 189.12340 | 1.4 | 1.6673 |
| Arg-Gln | Dipeptides | 1.025 | $C_{11}H_{22}N_6O_4$ | $[M+H]^+$ | 286.15097 | 286.15100 | −0.1 | 1.6572 |
| Phe-Pro | Dipeptides | 3.055 | $C_{14}H_{18}N_2O_3$ | $[M+H]^+$ | 263.13907 | 263.13901 | 0.2 | 1.6562 |
| Phytosphingosine | Phytosphingosines | 7.893 | $C_{18}H_{39}NO_3$ | $[M+H]^+$ | 318.30017 | 318.30020 | −0.1 | 1.6243 |
| 5-(Carbamoylamino)pentanoic acid | Amino acids | 2.226 | $C_6H_{12}N_2O_3$ | $[M+H]^+$ | 100.07606 | 100.07570 | 3.6 | 1.5755 |
| (Z)-3-Hexenylvicianoside | O-acyl carbohydrate | 4.237 | $C_{17}H_{30}O_{10}$ | $[M+H]^+$ | 412.21793 | 412.21799 | −0.1 | 1.5699 |
| 4-Methylamino-4-pyridin-3-ylbutanoic acid | Carboxyl acids | 2.563 | $C_{10}H_{14}N_2O_2$ | $[M+H]^+$ | 195.11305 | 195.11279 | 1.3 | 1.5554 |
| 2-Pyrrol-1-ylbenzoic acid | Carboxyl acids | 2.566 | $C_{11}H_9NO_2$ | $[M+H]^+$ | 188.07144 | 188.07060 | 4.5 | 1.5549 |
| 3-[(2S,5S)-5-(2-methylpropyl)-3,6-dioxopiperazin-2-yl]propanoic acid | Carboxyl acids | 2.616 | $C_{11}H_{18}N_2O_4$ | $[M+NH_4]^+$ | 243.13394 | 243.13390 | 0.2 | 1.5236 |
| Ala-Nle | Dipeptides | 2.097 | $C_9H_{18}N_2O_3$ | $[M+NH_4]^+$ | 203.13895 | 203.13901 | −0.3 | 1.5089 |
| *N*-Acetylleucine | Amino acids | 3.411 | $C_8H_{15}NO_3$ | $[M+H]^+$ | 174.11224 | 174.11230 | −0.3 | 1.4734 |
| PC(16:0–18:0) | Phospholipids | 13.303 | $C_{42}H_{80}NO_8P$ | $[M+H]^+$ | 780.55164 | 780.55139 | 0.3 | 1.4565 |
| Ile-Ala | Dipeptides | 1.954 | $C_9H_{18}N_2O_3$ | $[2M+H]^+$ | 203.13898 | 203.13901 | −0.1 | 1.4533 |
| 4-Oxobedfordiaic Acid | Sesquiterpenes | 2.107 | $C_{15}H_{22}O_3$ | $[M+H]^+$ | 273.14401 | 273.14600 | −7.3 | 1.4424 |
| *N*-Acetyltyramine | Biogenic monoamines | 3.050 | $C_{10}H_{13}NO_2$ | $[M+H]^+$ | 180.10194 | 180.10190 | 0.2 | 1.4384 |
| 3-Amino-L-tyrosine | Amino acids | 2.988 | $C_9H_{12}N_2O_3$ | $[M+H]^+$ | 393.17627 | 393.17691 | −1.6 | 1.4333 |
| L-Cysteine | Amino acids | 0.464 | $C_3H_7NO_2S$ | $[M+H]^+$ | 105.00085 | 105.00050 | 3.3 | 1.4317 |
| PyroGlu-Val | Dipeptides | 2.578 | $C_{10}H_{16}N_2O_4$ | $[M+K]^+$ | 229.11827 | 229.11830 | −0.1 | 1.4314 |
| γ-Glu-Glu | Dipeptides | 2.407 | $C_{10}H_{16}N_2O_7$ | $[M+K]^+$ | 260.07739 | 260.07651 | 3.4 | 1.4300 |
| γ-Glu-Phe | Dipeptides | 1.883 | $C_{14}H_{16}N_2O_4$ | $[M+K]^+$ | 277.11807 | 277.11829 | −0.8 | 1.4289 |
| *N*-Acetylphenylalanine | Amino acids | 3.880 | $C_{11}H_{13}NO_3$ | $[M+H]^+$ | 208.0966 | 208.09660 | 0.0 | 1.4199 |
| 6-Oxooctadecanoic acid | Medium and short-chain keto acids | 10.702 | $C_{18}H_{34}O_3$ | $[M+H]^+$ | 316.28479 | 316.28461 | 0.6 | 1.3920 |
| Ile-Ser | Dipeptides | 2.157 | $C_9H_{18}N_2O_4$ | $[M+Na]^+$ | 217.11902 | 217.11940 | −1.8 | 1.3857 |
| Leu-Glu | Dipeptides | 1.913 | $C_{11}H_{20}N_2O_5$ | $[M+Na]^+$ | 261.14471 | 261.14450 | 0.8 | 1.3560 |
| L-Homoserine | Amino acids | 2.413 | $C_4H_9NO_3$ | $[2M+K]^+$ | 237.10887 | 237.10921 | −1.4 | 1.3545 |
| *N*-(*tert*-Butoxycarbonyl)glycine | Amino acids | 2.388 | $C_7H_{13}NO_4$ | $[M+H]^+$ | 176.09175 | 176.09171 | 0.2 | 1.3386 |
| *N*-(2-Hydroxyethyl)iminodiacetic acid | Dicarboxilic acids | 0.476 | $C_6H_{11}NO_5$ | $[M+H]^+$ | 160.06079 | 160.06039 | 2.5 | 1.3136 |
| 3-Methyladipic acid | Dicarboxilic acids | 2.382 | $C_7H_{12}O_4$ | $[M+H]^+$ | 183.06261 | 183.06281 | −1.1 | 1.3110 |
| N-Acetyl-DL-valine | Amino acids | 2.692 | $C_7H_{13}NO_3$ | $[M+H]^+$ | 160.09645 | 160.09680 | −2.2 | 1.3057 |
| Tazettine | Alkaloids | 2.282 | $C_{18}H_{21}NO_5$ | $[M+H]^+$ | 332.15002 | 332.14926 | 2.3 | 1.3057 |

**Table 1.** *Cont.*

| Metabolite Name | Chemical Family | $R_t$ (min) | Formula | Adduct | Observed *m/z* | Calculated *m/z* | Error (ppm) | Cocoa Shell (Count × $10^4$) |
|---|---|---|---|---|---|---|---|---|
| Phe-Ile | Dipeptides | 2.282 | $C_{15}H_{22}N_2O_3$ | $[2M+Na]^+$ | 279.17029 | 279.17029 | 0.0 | 1.2998 |
| Ser-Leu | Dipeptides | 0.819 | $C_9H_{18}N_2O_4$ | $[M+H]^+$ | 219.134 | 219.13390 | 0.5 | 1.2740 |
| Leu-Val-Pro | Tripeptides | 3.077 | $C_{16}H_{29}N_3O_4$ | $[M+H]^+$ | 328.22336 | 328.22311 | 0.8 | 1.2653 |
| L-Homocitrulline | Amino acids | 1.921 | $C_7H_{15}N_3O_3$ | $[M+H]^+$ | 212.10071 | 212.10060 | 0.5 | 1.2619 |
| Ethyl L-leucinate | Amino acids | 2.338 | $C_7H_{15}NO_2$ | $[M+H]^+$ | 160.13255 | 160.13300 | −2.8 | 1.2483 |
| Linoleoyl ethanolamide | *N*-acylethanolamines | 10.574 | $C_{20}H_{37}NO_2$ | $[M+H]^+$ | 324.28983 | 324.28970 | 0.4 | 1.2458 |
| Methyl 3,4,5-trihydroxycyclohexene-1-carboxylate | Carbonyls | 1.753 | $C_8H_{12}O_5$ | $[M+H]^+$ | 230.10199 | 230.10201 | −0.1 | 1.2432 |
| PC (16:0/22:5) | Phospholipids | 11.864 | $C_{46}H_{82}NO_8P$ | $[M+H]^+$ | 830.56665 | 830.56702 | −0.4 | 1.2241 |
| Ala-Phe | Dipeptides | 2.523 | $C_{12}H_{16}N_2O_3$ | $[M+H]^+$ | 237.12341 | 237.12340 | 0.0 | 1.2230 |
| *trans*-Cinnamic acid | (Poly)phenols | 2.139 | $C_9H_8O_2$ | $[M+H]^+$ | 149.05951 | 149.05971 | −1.3 | 1.2199 |
| *O*-Benzyl-L-serine | Amino acids | 1.990 | $C_{10}H_{13}NO_3$ | $[M+H]^+$ | 196.09682 | 196.09680 | 0.1 | 1.2078 |
| 5-Methoxytryptophan | Amino acids | 2.198 | $C_{12}H_{14}N_2O_3$ | $[M+H]^+$ | 235.1078 | 235.10770 | 0.4 | 1.1960 |
| His-Thr-Lys | Tripeptides | 4.882 | $C_{16}H_{28}N_6O_5$ | $[M+Na]^+$ | 367.20892 | 367.20880 | 0.3 | 1.1949 |
| Scalusamide A | Pyrrolidines | 1.923 | $C_{16}H_{27}NO_3$ | $[M+K]^+$ | 304.18692 | 304.18799 | −3.5 | 1.1937 |
| Lys-Asn | Dipeptides | 2.072 | $C_{10}H_{20}N_4O_4$ | $[M+H]^+$ | 283.13898 | 283.13770 | 4.5 | 1.1887 |
| 2-Pyridinecarboxaldehyde | Pyridine | 0.602 | $C_6H_5NO$ | $[M+H]^+$ | 108.04469 | 108.04440 | 2.7 | 1.1767 |
| 4-(Butylamino)benzoic acid | Carbocyclic acids | 7.993 | $C_{11}H_{15}NO_2$ | $[M+H]^+$ | 194.11751 | 194.11760 | −0.5 | 1.1756 |
| Glu-Pro | Dipeptides | 0.941 | $C_{10}H_{14}N_2O_4$ | $[M+H]^+$ | 227.10255 | 227.10260 | −0.2 | 1.1669 |
| His-Pro | Dipeptides | 2.329 | $C_{11}H_{16}N_4O_3$ | $[M+H]^+$ | 253.12955 | 253.12950 | 0.2 | 1.1635 |
| Desmotroposantonin | Terpenes | 5.085 | $C_{15}H_{18}O_3$ | $[M+H]^+$ | 247.13298 | 247.13300 | −0.1 | 1.1550 |
| γ-Glu-Val | Dipeptides | 0.632 | $C_{10}H_{18}N_2O_5$ | $[M+H]^+$ | 247.20084 | 247.20000 | 3.4 | 1.1543 |
| MGDG O-8:0/2:0 | Galactolipids | 2.453 | $C_{19}H_{36}O_9$ | $[2M+H]^+$ | 431.22403 | 431.22516 | −2.6 | 1.1503 |
| L-Propionylcarnitine | Amino acids | 2.100 | $C_{10}H_{19}NO_4$ | $[M+H]^+$ | 240.11928 | 240.12061 | −5.5 | 1.1452 |
| *N*6-Succinyladenosine | Purine Nucleosides | 2.301 | $C_{14}H_{17}N_5O_8$ | $[M+K]^+$ | 384.11508 | 384.11499 | 0.2 | 1.1387 |
| *N*-α-Acetyl-L-arginine | Amino acids | 0.873 | $C_8H_{16}N_4O_3$ | $[2M+H]^+$ | 217.12956 | 217.12950 | 0.3 | 1.1374 |
| L-Citrulline | Amino acids | 0.543 | $C_6H_{13}N_3O_3$ | $[M+Na]^+$ | 159.07658 | 159.07640 | 1.1 | 1.1237 |
| Phe-Ala-Lys | Tripeptides | 2.583 | $C_{18}H_{28}N_4O_4$ | $[M+H]^+$ | 183.11249 | 183.11279 | −1.6 | 1.1080 |
| *N*5-(1-Iminoethyl)-L-ornithine | Amino acids | 1.895 | $C_7H_{15}N_3O_2$ | $[M+H]^+$ | 174.12317 | 174.12370 | −3.0 | 1.0954 |
| 7-Keto-8-aminopelargonic acid | Amino acids | 3.566 | $C_9H_{17}NO_3$ | $[M+NH_4]^+$ | 170.11769 | 170.11760 | 0.5 | 1.0777 |
| 4-Methyl-2-oxovaleric acid | Medium and short-chain keto acids | 2.632 | $C_6H_{10}O_3$ | $[M+H]^+$ | 113.05968 | 113.05970 | −0.2 | 1.0733 |
| Val-Trp | Dipeptides | 3.233 | $C_{16}H_{21}N_3O_3$ | $[M+Na]^+$ | 304.16547 | 304.16559 | −0.4 | 1.0630 |
| Glu-Ala-Lys | Tripeptides | 1.111 | $C_{14}H_{24}N_4O_5$ | $[M+H]^+$ | 329.18179 | 329.18188 | −0.3 | 1.0484 |
| O-Phospho-L-threonine | Amino acids | 0.575 | $C_4H_{10}NO_6P$ | $[M+K]^+$ | 222.01401 | 222.01379 | 1.0 | 1.0336 |
| *N*-Acetylmannosamine | Amino sugar | 2.389 | $C_8H_{15}NO_6$ | $[2M+NH_4]^+$ | 222.09795 | 222.09810 | −0.7 | 1.0325 |
| 2′-Deoxyuridine | Pyrimidine | 1.111 | $C_9H_{12}N_2O_5$ | $[M+H]^+$ | 211.07178 | 211.07130 | 2.3 | 1.0163 |
| Gly-Ile | Dipeptides | 0.811 | $C_8H_{16}N_2O_3$ | $[M+H]^+$ | 189.12372 | 189.12350 | 1.2 | 1.0063 |
| Leu-Leu | Dipeptides | 2.845 | $C_{12}H_{24}N_2O_3$ | $[M+H]^+$ | 245.186 | 245.18600 | 0.0 | 0.6975 |

SM: Sphingomyelin; PC: Phosphatidylcholine; MGDG: Monogalactosyldiacylglycerol; PE: Phosphatidylethanolamine; cAMP: Cyclic adenosine monophosphate.

The xanthines identified, mainly caffeine ($[M+H]^+$ = 195.08735 $m/z$) and theobromine ($[M+H]^+$ = 181.07198 $m/z$), are well-known for their roles in central nervous system stimulation, neurotransmitter regulation, and cognitive enhancement. Both compounds are also implicated in energy metabolism regulation, reinforcing the potential metabolic benefits of CSE. The presence of these compounds suggests both neurological and metabolic benefits, potentially contributing to enhanced cognitive function and metabolic activity. Additionally, other significant compounds included phenylethylamines (known for their stimulant and psychoactive properties, influencing mood and focus), pyridine carboxylic acids (which play important roles in vitamin B metabolism and overall energy production), dipeptides (such as Val-Val and Ile-Phe, which are involved in protein synthesis, cellular repair, and metabolism), amino fatty acids (important in maintaining membrane structure and signaling pathways), and carnitines (crucial for fatty acid metabolism and mitochondrial function, particularly in energy production through β-oxidation).

The analysis also detected pyrroline carboxylic acids (linked to the regulation of oxidative stress), quinolines (involved in various enzyme systems and redox reactions), and phytosphingosines (key mediators in lipid signaling pathways and cellular membrane stability). The detection of these compounds underlines the extract's potential to modulate oxidative stress responses and lipid homeostasis, further emphasizing its bioactive potential. These compounds, shown in Figure 2A, contribute to the rich biochemical diversity of CSE, and suggest multiple physiological roles that extend beyond primary metabolism. The metabolic pathway analysis revealed the significant involvement of key biochemical pathways, particularly those pathways associated with phenylalanine, caffeine, aminoacyl-tRNA biosynthesis, glycine, serine and threonine, and arginine and proline metabolism (Figure 2B).

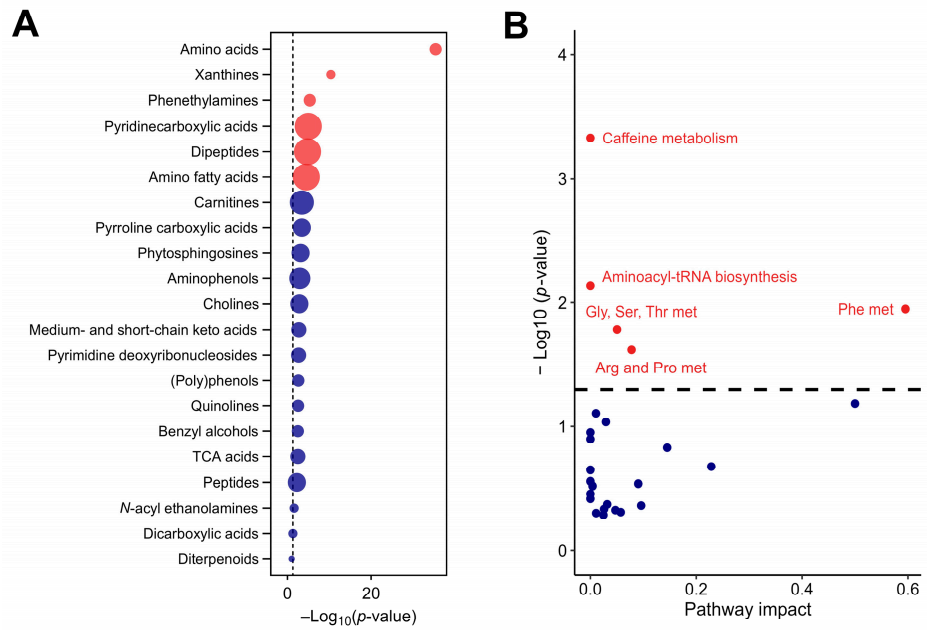


**Figure 2.** The chemical and functional composition of the cocoa shell extract (CSE), including metabolic pathways with significant impact, as identified by untargeted metabolomics (**A**) and enrichment analysis of subclass chemical structures (**B**), where the size of the dots indicates the enrichment ratio. Red dots indicate structures and pathways with significant differences, with *p*-values adjusted by the false discovery rate (FDR). Blue dots represent structures and pathways without significant differences. Gly, Ser, Thr met: glycine, serine, and threonine metabolism; Phe met: phenylalanine metabolism; Arg and Pro met: arginine and proline metabolism.

In addition to the pathway analysis, the network analysis (Figure 3) further elucidates the interconnections between metabolic pathways and individual metabolites identified in the CSE, offering insights into its potential bioactive applications. The network map underscores the central role of several key pathways, with phenylalanine metabolism ($p$ = 0.013) emerging as a core node. Phenylalanine and its downstream products, such as L-tyrosine and tyramine, are involved in the biosynthesis of neurotransmitters, particularly dopamine and norepinephrine, which are critical for cognitive functions such as mood regulation and mental alertness. This finding suggests that phenylalanine-related metabolites in CSE could confer neuroactive properties, potentially enhancing cognitive performance and alertness.

Arginine and proline metabolism ($p$ = 0.005) plays another critical role in the network, encompassing key metabolites like L-proline, L-citrulline, and L-arginine. These compounds are integral to protein synthesis, nitric oxide production, and the plant urea cycle. In humans, their well-known functions in vascular health, muscle metabolism, and recovery highlight the potential for CSE to be used in cardiovascular support and muscle recovery nutraceutical formulations. Notably, L-citrulline is associated with improved blood flow through its vasodilatory effects, underscoring the cardiovascular benefits that could be exploited from CSE-based products.

Caffeine metabolism ($p$ = 0.019) also forms a prominent and interconnected cluster, including caffeine, theobromine, and 7-methylxanthine. In *Theobroma cacao*, these xanthines contribute to plant defense and growth regulation, while in humans, they are recognized for their stimulatory effects on the central nervous system. Their potential to enhance cognitive alertness and physical endurance through mechanisms such as adenosine receptor inhibition and dopamine stimulation positions CSE as a promising natural source of energy-boosting nutraceuticals. The synergy between these xanthines could further amplify these stimulatory effects, reinforcing CSE's multifaceted role in enhancing cognitive and physical performance.

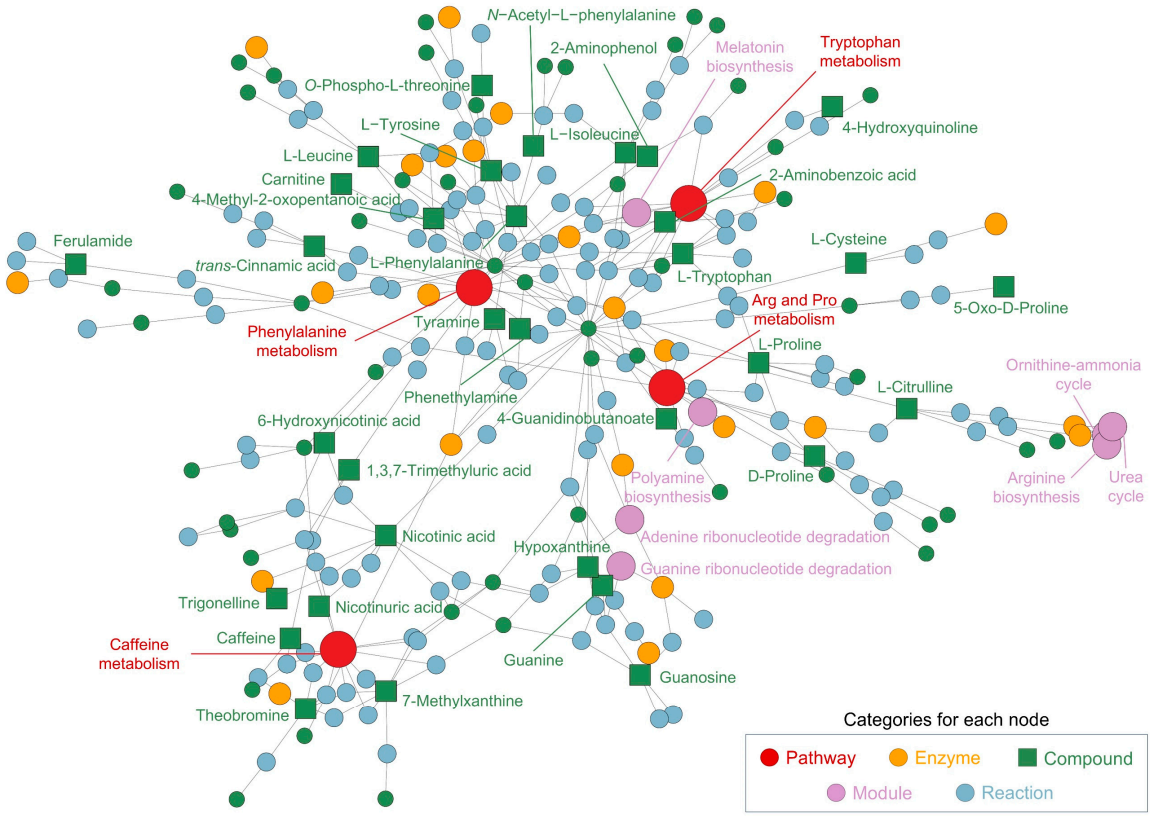


**Figure 3.** Network and pathway analysis of metabolites identified in the cocoa shell extract (CSE), illustrating the interconnected metabolic pathways and compounds. The network highlights significant metabolic pathways, including phenylalanine metabolism, arginine and proline metabolism, caffeine metabolism, and tryptophan metabolism. Nodes represent different categories: pathways (red, ●), enzymes (yellow, ●), compounds (green, ■), modules (purple, ●), and reactions (blue, ●). Arg and Pro metabolism: arginine and proline metabolism.

Other significant pathways include amino acid metabolism, such as glycine, serine, and threonine biosynthesis ($p = 0.041$), which is essential for protein turnover and cellular regeneration. The clustering of aminoacyl-tRNA biosynthesis within the network highlights CSE's potential to support protein synthesis, making it beneficial for muscle health and recovery. Additionally, pyridine carboxylic acid metabolism, including nicotinic acid and 6-hydroxynicotinic acid, suggests involvement in vitamin B3 metabolism ($p = 0.039$), a crucial process for maintaining cellular energy homeostasis and lipid metabolism. This connection indicates that CSE may help to support energy production and reduce oxidative stress. Moreover, the presence of quinoline derivatives and phytosphingosines in the network suggests additional layers of bioactivity. Quinoline derivatives, for instance, have been linked to enzyme regulation and antimicrobial activity, whereas phytosphingosines are involved in lipid signaling pathways crucial for maintaining skin barrier integrity. This further extends the possible applications of CSE beyond cognitive and cardiovascular benefits, potentially opening avenues for its use in cosmeceuticals or skincare formulations aimed at enhancing skin health. The metabolic pathways associated with caffeine metabolism, purine degradation ($p = 0.003$), and guanine ribonucleotide degradation ($p = 7.58 \times 10^{-5}$) further reveal CSE's role in energy and nucleotide metabolism, which are essential for maintaining cellular energy levels, proliferation, and overall metabolic balance. The creatine pathway ($p = 1.0 \times 10^{-6}$), essential for energy storage in muscle and brain tissues, highlights another potential use of CSE in performance-enhancing supplements or recovery aids. Furthermore, ceramide ($p = 0.028$) and sphingosine ($p = 0.026$) biosynthesis

pathways indicate CSE's potential to regulate lipid metabolism and support skin health, reinforcing its bioactive versatility.

Altogether, this comprehensive network of metabolic pathways and compounds in cocoa shell points to various potential health benefits, from neurotransmitter regulation and cardiovascular support, to skin health and metabolic balance. The compounds and pathways identified in the network underscore the multifunctional nature of CSE, supporting its use in a diverse range of nutraceutical products aimed at enhancing cognitive performance, cardiovascular health, muscle recovery, and general metabolic well-being. By leveraging the interconnected nature of these bioactive compounds, CSE could offer synergistic benefits, making it a highly versatile ingredient for nutraceutical and cosmeceutical formulations. Therefore, the metabolomic profiling of CSE provides a comprehensive overview of its chemical composition, revealing a variety of bioactive compounds with potential physiological effects. Integrating both pathway and network analysis further emphasizes CSE's potential for having significant impacts on neurological, cardiovascular, and metabolic processes, supporting its potential use in nutraceutical formulations targeting cognitive function, energy metabolism, and vascular health.

### *3.2. Chemometric Analysis of Rat Plasma Metabolome Revealed Distinct Metabolic Profiles During CSE Supplementation*

Throughout the supplementation period, a total of 244 metabolites were detected in rat plasma. Of these, 84.8% were detected at baseline, 91.8% on day 4, and notably fewer, 68.0%, on day 7, indicating dynamic metabolic adjustments throughout supplementation. The chemometric analysis of the untargeted metabolomic data revealed distinct changes in the rat plasma metabolome following CSE supplementation. PCA indicated that components 1 and 2 accounted for 51.3% of the total variance, with a discernible clustering of metabolites, denoting significant metabolic shifts. Specifically, samples from the baseline and day 4 time points were grouped closely, while those from day 7 formed a distinct cluster, demonstrating a marked shift in the metabolic profile by this time point (Figure 4A).

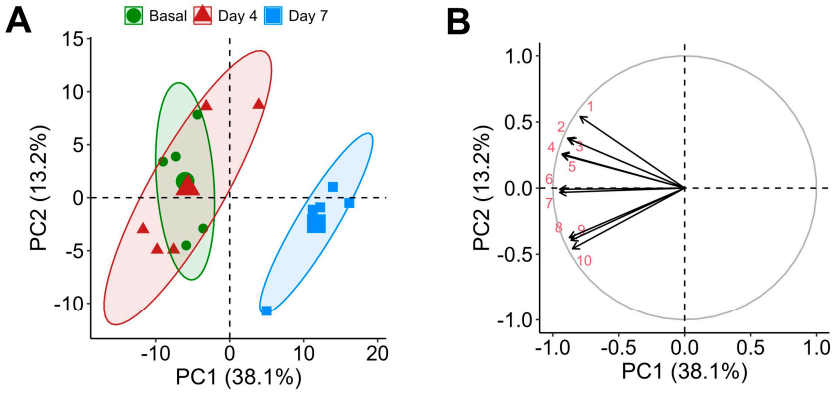


**Figure 4.** Principal Component Analysis (PCA) of the plasma metabolome with cocoa shell extract (CSE) supplementation, showing a PCA scores plot illustrating the separation of samples by time points: baseline (green circles, ●), day 4 (red triangles, ▲), and day 7 (blue squares, ■) (**A**), and a loadings plot highlighting the main metabolites contributing to the variance (**B**). Principal components (PCs): 1: ceramide 8:0;2O/14:0; 2: 12-(3-(Adamantan-1-yl)ureido)dodecanoic acid; 3: 6-Hydroxy-5a-methyl-3,9-dimethylidenedecahydronaphtho[1,2-b]furan-2(3h)-one; 4: L-Leucyl-L-alanine; 5: Octapamine; 6: 1-Myristoyl-sn-glycero-3-phosphocholine; 7: Monoacylglycerophosphocholines 18:3; 8: 1-alkyl,2-acylglycerophosphocholines 20:4; 9: 1-alkyl,2-acylglycerophosphocholines 16:0; 10: Monoacylglycerophosphocholines 22:6.

This clustering indicates a time-dependent metabolic response to CSE supplementation. The 10 uppermost influential metabolites in the PCA were mainly lipids, including

contributions from ceramides (ceramide 8:0;2O/14:0) and glycerophosphocholine derivatives (1-myristoyl-sn-glycero-3-phosphocholine, LPC 18:3, LPC 22:6, PC O-20:4, PC O-16:0), reflecting significant lipidomic alterations, which may influence changes in membrane fluidity, signaling, or energy metabolism. Additionally, metabolites like 12-(3-(adamantan-1-yl)ureido)dodecanoic acid and octapamine were highlighted, underscoring potential modifications in fatty acid metabolism and alteration of neurotransmitter precursor levels, respectively. Other compounds contributing to the variance included 6-hydroxy-5a-methyl-3,9-dimethylidenedecahydronaphtho[1,2-b]furan-2(3h)-one, a soluble epoxide hydrolase enzyme inhibitor (a compound potentially linked to (poly)phenol metabolism and associated with antioxidant properties), and the dipeptide L-leucyl-L-alanine (indicative of altered peptide metabolism) (Figure 4B). These findings suggest that lipid and amino acid metabolism is particularly responsive to CSE supplementation.

The heatmap analysis further illustrated the temporal changes in the metabolome, where the metabolic fingerprint at the basal time point displayed only subtle differences compared to day 4. However, a pronounced divergence emerged by day 7, indicating that significant metabolic shifts had occurred over the course of the 7-day CSE supplementation (Figure 5). These shifts are visually represented by the increasing intensity of red and blue signals, especially by day 7, reflecting upregulated and downregulated metabolites, respectively. This observation suggests that the rat metabolome underwent a progressive reconfiguration over time, with minimal metabolic perturbations during the first 4 days of CSE exposure. The distinct clustering of samples from day 7 highlights a clear separation from both the basal and day 4 samples. This temporal progression implies that longer exposure to CSE is required to induce significant metabolic alterations. While the early metabolic response (day 4) appears to be more similar to the basal state, it is at day 7 that the most pronounced metabolic changes are observed. As a result, the data from day 4 were considered not substantially different from the baseline, and were subsequently excluded from further differential analysis. The heatmap reveals that several metabolites showed consistent changes by day 7, indicated by the tightly grouped red and blue patterns, suggesting potential biomarkers or key metabolites influenced by the CSE supplementation.

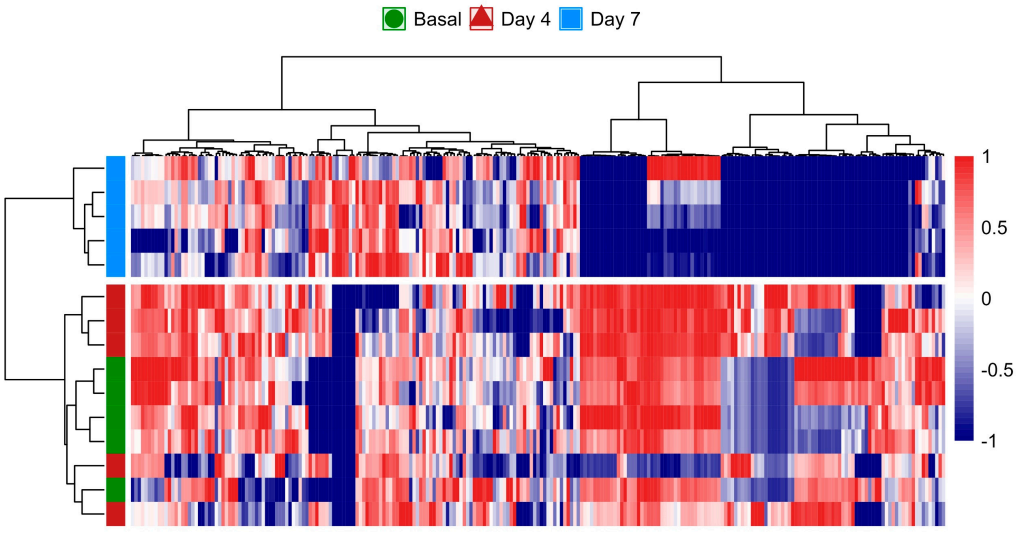


**Figure 5.** Heatmap analysis of the rat plasma metabolome over the 7-day CSE supplementation period, illustrating the progressive reconfiguration of metabolic profiles. The color scale from blue to red represents the relative intensity of metabolite levels, with blue indicating lower levels and red indicating higher levels. Hierarchical clustering on both axes shows the relationships and grouping patterns among the metabolites and time points, highlighting significant metabolic shifts by day 7.

These alterations provide insights into the time-dependent effects of CSE on the metabolic profile, showing that prolonged exposure is necessary to elicit significant biological responses. The hierarchical clustering of the samples also demonstrates that metabolic responses were relatively consistent within each time point (day 0, day 4, and day 7). However, the most substantial metabolic deviation occurs between day 7 and the earlier time points, confirming CSE's delayed but significant metabolic impact.

To further explore the metabolic changes and bioavailability of compounds introduced through CSE, the Venn diagram (Figure 6) illustrates the distribution of these metabolites, highlighting how the CSE contributes a unique set of compounds to the plasma after supplementation. These findings emphasize the importance of understanding the metabolites present in dietary supplements, their bioavailability, and their potential physiological relevance. The chemometric analysis underscores that while many metabolites in CSE do not directly appear in plasma, those that are bioavailable could play critical roles in driving the supplement's health benefits. Interestingly, a significant portion of the metabolites identified in CSE (84.2%) were unique to the extract and undetectable in plasma both before and after supplementation. This suggests that many of the CSE's components were either not absorbed or rapidly metabolized into other compounds post-ingestion. Understanding bioavailability (the extent and rate at which ingested compounds enter the systemic circulation and are available for biological activity) is essential when evaluating the efficacy of dietary supplements, as only bioavailable compounds can exert physiological effects. From the total metabolites identified, only 21 compounds (5.6%) were consistently found across all groups: the CSE, the plasma at baseline (basal), and after 7 days of supplementation (day 7). This small subset of metabolites suggests that only a limited fraction of the compounds present in the CSE circulate consistently in the bloodstream, both before and after supplementation. Among these, only three compounds (0.8% of all compounds found, 1.7% of CSE's metabolites) were bioavailable after supplementation, being absent in the basal state but detectable on day 7. These bioavailable compounds, *N*-isovaleroylglycine ($[M+H]^+$ = 160.09671 $m/z$), caffeine ($[M+H]^+$ = 195.08735 $m/z$), and theobromine ($[M+H]^+$ = 181.07198 $m/z$), are of particular interest because of their known physiological effects. Caffeine and theobromine, two well-known stimulants, are associated with increased alertness, cognitive performance, and physical endurance. Meanwhile, *N*-isovaleroylglycine, a lesser-known metabolite, has been linked to metabolic processes, suggesting potential impacts on amino acid and protein metabolism. Although the number of bioavailable compounds is relatively low, their physiological implications could be significant, particularly in enhancing cognitive function and energy metabolism. The Venn diagram (Figure 6) also shows that 130 compounds (34.8%) were shared between the basal state and day 7, suggesting that these metabolites are endogenous and unaffected by CSE supplementation. The presence of 12 unique compounds (3.2%) detectable only on day 7, and 52 compounds (13.9%) unique to the basal state, further underscores the dynamic nature of the plasma metabolome and the metabolic shifts induced by CSE supplementation. These findings highlight the importance of the bioavailable compounds and the broader metabolic changes driven by CSE. The chemometric analysis revealed that CSE supplementation induced dynamic shifts, particularly in lipid and amino acid metabolism, with the bioavailability of key compounds like caffeine and theobromine standing out. This underscores CSE's potential physiological impacts, particularly in cognitive enhancement and energy metabolism, while also pointing to areas where CSE's influence may remain undetected due to rapid metabolism or limited absorption.

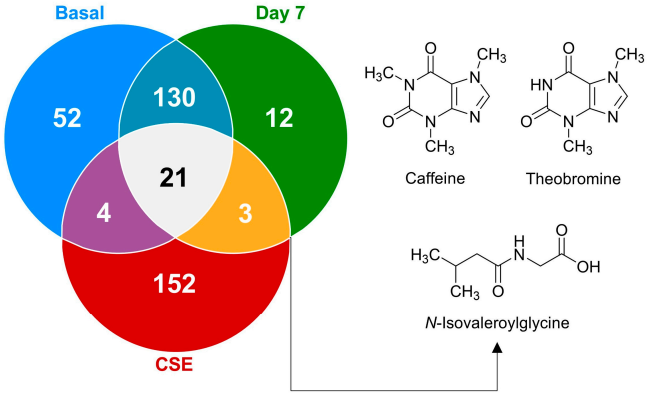


**Figure 6.** A Venn diagram illustrating the distribution of shared and unique metabolites at the basal time point, on day 7, and after cocoa shell extract (CSE) administration. The metabolites present on day 7 but absent at basal are depicted, highlighting their potential as bioactive compounds derived from CSE.

### *3.3. Dynamic Modulation of Metabolic Pathways Induced by CSE Supplementation Was Observed by Pathway Analysis*

Initially, 23 signaling pathways were identified at the basal time point, which increased slightly to 24 by day 7. At the basal time point, the main pathways with significant impact were those related to the metabolism of phenylalanine, tryptophan, aminoacyl-tRNA biosynthesis, glutathione, arginine and proline, nicotinate and nicotinamide, glycine, serine and threonine, and glycerophospholipid (Figure 7A). By day 7, the metabolic pathways that maintained their impact were those related to phenylalanine, aminoacyl-tRNA biosynthesis, and glycine, serine, and threonine. These pathways are essential for protein synthesis and overall cellular function. Those that had increased impact were related to glycerophospholipid, nicotinate, and nicotinamide metabolism, suggesting augmented lipid remodeling and energy homeostasis processes. Conversely, the pathways that showed decreased impact were tryptophan, glutathione, arginine, and proline metabolism, indicating changes in amino acid metabolism and cellular antioxidant capacity. Additionally, new metabolic activity was detected in the pyrimidine and caffeine metabolism pathways, suggesting the introduction of CSE components into the host metabolism (Figure 7B).

The semi-quantitative changes revealed that 74 out of 244 metabolites showed a significant fold change from basal to day 7. The majority (58 metabolites) exhibited a decrease, while 16 showed an increase (Table 2). Supplementary Table S2 provides the key metabolites detected in rat plasma after cocoa shell extract supplementation, their associated metabolic pathways, and their potential health effects. Certain metabolites stood out due to their significant fold changes among the dynamic alterations reported in metabolic pathways after CSE administration. The 3.5-fold drop in levels of docosahexaenoic acid (DHA) methyl ester ($[M+H]^+$ = 343.26376 $m/z$), and the 635.1-fold drop in PC O-20:5 ($[M+H]^+$ = 522.35655 $m/z$), a phosphatidylcholine-containing eicosapentaenoic acid (EPA), might indicate higher usage or altered metabolism of omega-3 fatty acids, which are essential for brain function and have anti-inflammatory effects. Compounds related to cellular maintenance and stress response also showed significant decreases; spermidine ($[M+NH_4]^+$ = 146.16516 $m/z$) decreased by 2.7-fold, potentially impacting cellular proliferation and longevity, while corticosterone ($[M+Na]^+$ = 347.22122 $m/z$) decreased by 3.0-fold, indicating a stress axis modulation. Similarly, a 2.8-fold drop in uric acid ($[M+H]^+$ = 169.03545 $m/z$) might reflect changes in oxidative stress management and purine breakdown. Moreover, decreases of 1.4- and 1.5-fold in tyrosine ($[M+H]^+$ = 182.08156 $m/z$) and creatine ($[M+NH_4]^+$ = 132.07704 $m/z$), respectively, both of which are required for neurotransmitter generation and energy storage, may indicate

changes in cognitive functioning and energy dynamics. In contrast, significant increases in metabolites such as *N*-[4-(methylthio)phenyl]-*N*′-phenylurea ([M+Na]$^+$ = 517.17255 $m/z$), which increased by 21.5-fold, and LPC O-13:1 ([M+H]$^+$ = 438.29791 $m/z$), which increased by 7.5-fold, indicate activation of detoxification mechanisms and changes in cell membrane dynamics. Furthermore, a 2.5-fold increase in caffeine ([M+H]$^+$ = 195.08792 $m/z$) and a 2.9-fold increase in theobromine ([M+H]$^+$ = 181.07225 $m/z$) highlight CSE's stimulatory effect, which may improve alertness and influence metabolic rate.

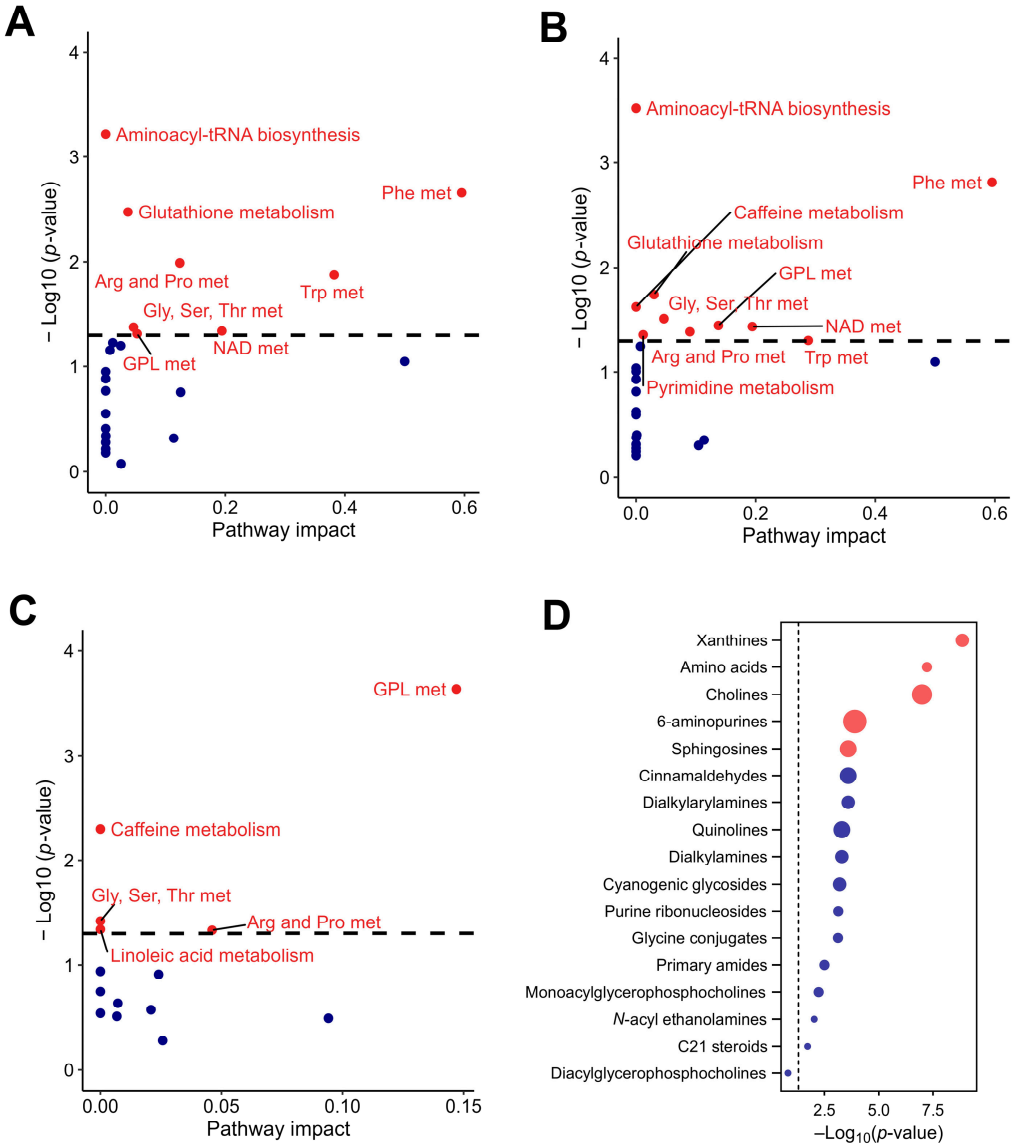


**Figure 7.** Pathway analysis of the rat plasma metabolome in response to CSE supplementation, including the metabolic pathways with significant impact at the basal time point (**A**), the metabolic pathways with significant impact at day 7 of CSE supplementation (**B**), the rat plasma pathways showing significant fold changes during the supplementation period (**C**), and a dot plot of the sub-classes of chemical structures showing significant enrichment ratios (**D**). Red dots indicate pathways with significant differences, with *p*-values adjusted by false discovery rate (FDR), while blue dots indicate pathways without significant differences. Gly, Ser, Thr met: glycine, serine, and threonine metabolism; Phe met: phenylalanine metabolism; NAD met: nicotinate and nicotinamide metabolism; Arg and Pro met: arginine and proline metabolism; Trp met: tryptophan metabolism; GLP met: glycerphospholipid metabolism.

**Table 2.** Differentially abundant metabolites in plasma following CSE Supplementation. This table presents the metabolites identified through untargeted metabolomic analysis, highlighting their retention time ($R_t$), molecular formula, adduct type, observed and calculated mass-to-charge ratios ($m/z$), mass error (in ppm), relative intensity (counts $\times$ $10^4$), fold change (FC) between basal and day 7 measurements, $p$-value, and false discovery rate (FDR). The data emphasize significant metabolic changes over the CSE supplementation period, providing insights into the compounds that exhibit differential abundance.

| Metabolite Name | $R_t$ (min) | Formula | Adduct | Observed $m/z$ | Calculated $m/z$ | Error (ppm) | Relative Intensity (Counts $\times$ $10^4$) | | FC | $p$-Value | FDR |
|---|---|---|---|---|---|---|---|---|---|---|---|
| | | | | | | | Basal | Day 7 | | | |
| 1-(4-methylsulfanylphenyl)-3-phenylurea | 8.378 | $C_{14}H_{14}N_2OS$ | $[M+Na]^+$ | 517.17255 | 517.17267 | −0.2 | 0.07 (0.00) | 1.86 (0.10) | 21.5 | 0.005 | 0.017 |
| LPC O-13:1 | 10.451 | $C_{21}H_{44}NO_6P$ | $[M+H]^+$ | 438.29791 | 438.29791 | 0.0 | 0.17 (0.00) | 1.36 (0.23) | 7.5 | 0.005 | 0.017 |
| 1-(2-Hydroxyethyl)-2,2,6,6-tetramethyl-4-piperidinol | 1.224 | $C_{11}H_{23}NO_2$ | $[M+H]^+$ | 202.18022 | 202.18021 | 0.0 | 0.23 (0.00) | 1.76 (0.30) | 6.9 | 0.005 | 0.017 |
| 1,2,3,4-Tetrahydro-b-carboline | 3.460 | $C_{11}H_{12}N_2$ | $[M+H]^+$ | 173.10725 | 173.10730 | −0.3 | 0.22 (0.00) | 1.34 (0.32) | 6.0 | 0.005 | 0.017 |
| PC (18:0/22:6) | 12.403 | $C_{48}H_{84}NO_8P$ | $[M+H]^+$ | 834.60095 | 834.60071 | 0.3 | 0.20 (0.00) | 0.70 (0.19) | 5.5 | 0.005 | 0.017 |
| 13-hydroperoxy-1-piperidin-1-ylicosa-2,4,14-trien-1-one | 12.591 | $C_{25}H_{43}NO_3$ | $[M+Na]^+$ | 406.32959 | 406.33099 | −3.4 | 1.03 (0.00) | 5.31 (0.81) | 4.6 | 0.005 | 0.017 |
| D-erythro-*N*-stearoylsphingosine | 8.203 | $C_{18}H_{37}NO_2$ | $[M+H]^+$ | 300.28961 | 300.28970 | −0.3 | 0.40 (0.00) | 1.16 (0.50) | 4.1 | 0.005 | 0.017 |
| DGGA 13:0/27:0 | 5.913 | $C_{49}H_{92}O_{11}$ | $[M+H]^+$ | 874.69995 | 874.69781 | 2.4 | 0.28 (0.00) | 0.88 (0.12) | 3.8 | 0.005 | 0.017 |
| Glucose | 2.619 | $C_6H_{12}O_6$ | $[M+K]^+$ | 181.07214 | 181.07204 | 0.6 | 0.32 (0.00) | 1.13 (0.15) | 3.8 | 0.005 | 0.017 |
| Docosahexaenoic acid methyl ester | 12.889 | $C_{23}H_{34}O_2$ | $[M+H]^+$ | 343.26376 | 343.26321 | 1.6 | 0.32 (0.00) | 1.19 (0.06) | 3.5 | 0.005 | 0.017 |
| NAGlySer 26:7/17:2 | 11.875 | $C_{48}H_{74}N_2O_7$ | $[M+H]^+$ | 808.58398 | 808.58344 | 0.7 | 0.74 (0.00) | 2.13 (1.03) | 3.0 | 0.019 | 0.050 |
| Theobromine | 2.391 | $C_7H_8N_4O_2$ | $[M+H]^+$ | 181.07225 | 181.07204 | 1.2 | 8.12 (0.00) | 24.5 (2.30) | 2.9 | 0.005 | 0.017 |
| *N*-Isovaleroylglycine | 2.376 | $C_7H_{13}NO_3$ | $[M+H]^+$ | 182.07898 | 182.07880 | 1.0 | 0.68 (0.17) | 1.98 (0.17) | 2.8 | 0.005 | 0.017 |
| Tripropylene glycol | 3.240 | $C_9H_{20}O_4$ | $[M+H]^+$ | 193.14313 | 193.14340 | −1.4 | 0.52 (1.42) | 2.86 (0.75) | 2.7 | 0.016 | 0.045 |
| Caffeine | 3.064 | $C_8H_{10}N_4O_2$ | $[M+H]^+$ | 195.08792 | 195.08771 | 1.1 | 4.91 (0.00) | 12.0 (0.55) | 2.5 | 0.005 | 0.017 |
| Choline cation | 0.569 | $C_5H_{14}NO$ | $[Cat]^+$ | 104.10635 | 104.10700 | −6.2 | 11.0 (0.60) | 17.4 (2.05) | 1.5 | 0.016 | 0.045 |
| 2-Methylisoquinolin-2-ium cation | 2.131 | $C_{10}H_{10}N$ | $[Cat-C_2H_3N]^+$ | 103.05445 | 103.05420 | 2.4 | 3.20 (0.25) | 2.90 (0.05) | −1.1 | 0.016 | 0.045 |
| Cytidine | 0.981 | $C_9H_{13}N_3O_5$ | $[M+H-C_5H_8O_4]^+$ | 112.05074 | 112.05050 | 2.1 | 11.8 (0.15) | 10.8 (0.35) | −1.1 | 0.009 | 0.027 |
| Tyrosine | 1.379 | $C_9H_{11}NO_3$ | $[M+H]^+$ | 182.08156 | 182.08141 | 0.8 | 9.29 (0.30) | 6.12 (0.42) | −1.4 | 0.016 | 0.045 |
| Asp-Lys | 0.599 | $C_{10}H_{19}N_3O_5$ | $[M+H]^+$ | 132.07436 | 132.07491 | −4.2 | 8.21 (0.52) | 5.42 (0.69) | −1.5 | 0.016 | 0.045 |
| Creatine | 0.716 | $C_4H_9N_3O_2$ | $[M+NH_4]^+$ | 132.07704 | 132.07727 | −1.7 | 3.54 (0.34) | 2.33 (0.34) | −1.5 | 0.016 | 0.045 |
| 7H-[1,2,4]Triazolo[4,3-b][1,2,4]triazole-3,7-diamine | 0.648 | $C_3H_5N_7$ | $[M+Na]^+$ | 140.0679 | 140.06790 | 0.0 | 2.85 (1.10) | 2.11 (0.11) | −1.5 | 0.009 | 0.027 |
| Emetine N-oxide | 0.612 | $C_{29}H_{40}N_2O_5$ | $[M+H]^+$ | 249.15613 | 249.15414 | 8.0 | 6.46 (0.30) | 3.88 (0.40) | −1.7 | 0.009 | 0.027 |
| Carbamazepine 10,11-epoxide | 1.516 | $C_{15}H_{12}N_2O_2$ | $[M+H]^+$ | 236.07085 | 236.07060 | 1.1 | 1.45 (0.06) | 0.63 (0.00) | −2.3 | 0.005 | 0.017 |
| Leu-Ala | 2.480 | $C_9H_{16}N_2O_2$ | $[M+H]^+$ | 185.12831 | 185.12840 | −0.5 | 1.04 (0.07) | 0.44 (0.00) | −2.4 | 0.005 | 0.017 |
| Quinoline | 2.561 | $C_9H_7N$ | $[M+H]^+$ | 130.0654 | 130.06512 | 2.2 | 1.09 (0.04) | 0.40 (0.00) | −2.6 | 0.005 | 0.017 |
| Spermidine | 0.470 | $C_7H_{19}N_3$ | $[M+NH_4]^+$ | 146.16516 | 146.16518 | −0.1 | 1.95 (0.46) | 0.76 (0.00) | −2.7 | 0.005 | 0.017 |
| SPB 19:0;2O | 7.998 | $C_{19}H_{41}NO_2$ | $[M+H]^+$ | 316.32098 | 316.32101 | −0.1 | 1.06 (0.23) | 0.41 (0.00) | −2.8 | 0.005 | 0.017 |
| Uric acid | 1.064 | $C_5H_4N_4O_3$ | $[M+H]^+$ | 169.03545 | 169.03560 | −0.9 | 1.45 (0.33) | 0.48 (0.00) | −2.8 | 0.005 | 0.017 |
| (2E,6E,12E)-19-(2-amino-2-oxoethyl)-9,11-dihydroxy-8-methoxy-10,12,14-trimethyl-15-oxohenicosa-2,6,12-trienedioic acid | 10.604 | $C_{27}H_{43}NO_9$ | $[M+H]^+$ | 543.32605 | 543.32800 | −3.6 | 1.15 (0.07) | 0.38 (0.00) | −2.9 | 0.005 | 0.017 |
| Corticosterone | 5.798 | $C_{21}H_{30}O_4$ | $[M+Na]^+$ | 347.22122 | 347.22131 | −0.3 | 2.10 (0.25) | 0.74 (0.00) | −3.0 | 0.005 | 0.017 |
| DL-Octopamine | 1.377 | $C_8H_{11}NO_2$ | $[M+H-H_2O]^+$ | 136.07574 | 136.07570 | 0.3 | 1.36 (0.01) | 0.40 (0.00) | −3.3 | 0.005 | 0.017 |
| 5-S-Methylthioadenosine | 2.576 | $C_{11}H_{15}N_5O_3S$ | $[M+H]^+$ | 298.09634 | 298.09683 | −1.6 | 0.95 (0.20) | 0.29 (0.00) | −3.7 | 0.005 | 0.017 |
| AUDA | 5.668 | $C_{23}H_{40}N_2O_3$ | $[M+H]^+$ | 216.1956 | 216.19580 | −0.9 | 1.31 (0.77) | 0.28 (0.00) | −4.2 | 0.005 | 0.017 |
| (R)-Prunasin | 3.286 | $C_{14}H_{17}NO_6$ | $[M+H]^+$ | 340.10226 | 340.10379 | −4.5 | 0.83 (0.53) | 0.26 (0.00) | −4.3 | 0.005 | 0.017 |
| 2,2,6,6-Tetramethyl-4-piperidinyl 2-methylacrylate | 6.097 | $C_{13}H_{23}NO_2$ | $[M+NH_4]^+$ | 226.18021 | 226.18021 | 0.0 | 5.22 (3.65) | 0.98 (0.00) | −5.0 | 0.005 | 0.017 |
| Leu-Pro | 1.997 | $C_{11}H_{20}N_2O_3$ | $[M+NH_4]^+$ | 229.1545 | 229.15469 | −0.8 | 1.37 (0.15) | 0.25 (0.00) | −5.1 | 0.005 | 0.017 |
| Jasminoside | 6.098 | $C_{15}H_{20}O_3$ | $[M+Na]^+$ | 266.17273 | 266.17380 | −4.0 | 3.54 (1.24) | 0.59 (0.00) | −5.2 | 0.005 | 0.017 |
| Kynurenine | 2.096 | $C_{10}H_{12}N_2O_3$ | $[M+NH_4]^+$ | 209.09207 | 209.09207 | 0.0 | 1.50 (0.55) | 0.25 (0.00) | −6.0 | 0.005 | 0.017 |
| 3-(4-hydroxy-3-methoxyphenyl)prop-2-enamide | 3.386 | $C_{10}H_{11}NO_3$ | $[M+H]^+$ | 194.08073 | 194.08099 | −1.3 | 1.11 (0.39) | 0.19 (0.00) | −6.3 | 0.005 | 0.017 |
| Diisooctyl phthalate | 12.351 | $C_{24}H_{38}O_4$ | $[M+Na]^+$ | 408.30878 | 408.31079 | −4.9 | 7.37 (3.06) | 1.09 (0.00) | −6.3 | 0.005 | 0.017 |
| 2-(1′,2′,3′,4′-Tetrahydroxybutyl)quinoxaline | 3.585 | $C_{12}H_{14}N_2O_4$ | $[M+H]^+$ | 251.10272 | 251.10260 | 0.5 | 1.66 (0.56) | 0.15 (0.00) | −10.1 | 0.005 | 0.017 |
| Spiroxamine | 9.949 | $C_{18}H_{35}NO_2$ | $[M+H]^+$ | 298.27356 | 298.27399 | −1.4 | 1.60 (1.24) | 0.12 (0.00) | −10.6 | 0.005 | 0.017 |
| Cer 8:0;2O/14:0 | 9.918 | $C_{22}H_{45}NO_3$ | $[M+H]^+$ | 372.34747 | 372.34723 | 0.6 | 1.18 (0.79) | 0.10 (0.00) | −14.5 | 0.005 | 0.017 |
| 1-(Cyclohexylmethyl)proline | 5.505 | $C_{12}H_{21}NO_2$ | $[M+NH_4]^+$ | 212.16447 | 212.16451 | −0.2 | 1.75 (2.03) | 0.11 (0.00) | −17.6 | 0.005 | 0.017 |

**Table 2.** *Cont.*

| Metabolite Name | $R_t$ (min) | Formula | Adduct | Observed *m/z* | Calculated *m/z* | Error (ppm) | Relative Intensity (Counts × $10^4$) | | FC | *p*-Value | FDR |
|---|---|---|---|---|---|---|---|---|---|---|---|
| | | | | | | | Basal | Day 7 | | | |
| Sydonic acid | 4.149 | $C_{15}H_{22}O_4$ | $[M+NH_4]^+$ | 266.15985 | 266.16000 | −0.6 | 1.91 (0.45) | 0.09 (0.00) | −19.7 | 0.005 | 0.017 |
| Adenine | 4.149 | $C_5H_5N_5$ | $[M+Na]^+$ | 271.11545 | 271.11630 | −3.1 | 1.74 (0.41) | 0.08 (0.00) | −19.9 | 0.005 | 0.017 |
| Icaridin | 5.506 | $C_{12}H_{23}NO_3$ | $[M+H]^+$ | 230.17514 | 230.17509 | 0.2 | 3.79 (4.19) | 0.22 (0.00) | −19.9 | 0.007 | 0.023 |
| Pentyl-b-D-glucopyranoside | 4.149 | $C_{11}H_{22}O_6$ | $[M+H]^+$ | 249.13336 | 249.13440 | −4.2 | 3.14 (1.39) | 0.13 (0.00) | −22.0 | 0.005 | 0.017 |
| (2R)-*N*-(3-Ethoxypropyl)-2,4-dihydroxy-3,3-dimethylbutanamide | 4.880 | $C_{11}H_{23}NO_4$ | $[M+H]^+$ | 216.15933 | 216.15939 | −0.3 | 2.01 (2.49) | 0.09 (0.00) | −25.7 | 0.005 | 0.017 |
| 7-Keto-8-aminopelargonic acid | 3.563 | $C_9H_{17}NO_3$ | $[M+H]^+$ | 188.12801 | 188.12810 | −0.5 | 5.46 (7.53) | 0.19 (0.00) | −31.8 | 0.005 | 0.017 |
| Phosphorylcholine | 10.271 | $C_5H_{14}NO_4P$ | $[M+H]^+$ | 184.07349 | 184.07332 | 0.9 | 1.29 (0.09) | 0.03 (0.00) | −45.1 | 0.005 | 0.017 |
| Phosphocholine | 10.093 | $C_5H_{14}NO_4P$ | $[M+H]^+$ | 184.073 | 184.07300 | 0.0 | 1.12 (0.27) | 0.03 (0.00) | −48.1 | 0.005 | 0.017 |
| Cer 8:1;2O/2:0 | 4.228 | $C_{10}H_{19}NO_3$ | $[M+H]^+$ | 202.14378 | 202.14377 | 0.0 | 1.62 (1.81) | 0.03 (0.00) | −53.7 | 0.005 | 0.017 |
| Triphenylphosphine oxide | 6.829 | $C_{18}H_{15}OP$ | $[M+H]^+$ | 279.09348 | 279.09329 | 0.7 | 1.05 (1.97) | 0.02 (0.00) | −59.7 | 0.005 | 0.017 |
| Cyclo(L-Leu-L-Pip-L-Aoe-D-Phe) | 9.824 | $C_{31}H_{44}N_4O_6$ | $[M+H]^+$ | 603.29346 | 603.29547 | −3.3 | 2.34 (0.27) | 0.04 (0.00) | −61.3 | 0.005 | 0.017 |
| *N*-cis-Hexadec-9-enoyl-L-homoserine lactone | 8.009 | $C_{20}H_{35}NO_3$ | $[M+H]^+$ | 338.26685 | 338.26901 | −6.4 | 2.42 (2.35) | 0.04 (0.00) | −65.0 | 0.005 | 0.017 |
| Methyprylon | 4.229 | $C_{10}H_{17}NO_2$ | $[M+H]^+$ | 184.13274 | 184.13280 | −0.3 | 1.11 (1.51) | 0.02 (0.00) | −74.2 | 0.005 | 0.017 |
| Melophlin D/H/I/J | 7.821 | $C_{20}H_{35}NO_3$ | $[M+Na]^+$ | 338.26645 | 338.26700 | −1.6 | 1.43 (1.54) | 0.02 (0.00) | −77.6 | 0.005 | 0.017 |
| 6-Oxooctadecanoic acid | 8.010 | $C_{18}H_{34}O_3$ | $[M+H]^+$ | 316.28479 | 316.28461 | 0.6 | 3.60 (3.53) | 0.04 (0.00) | −89.9 | 0.005 | 0.017 |
| Palmitoleoyl ethanolamide | 9.066 | $C_{18}H_{35}NO_2$ | $[M+NH_4]^+$ | 280.26373 | 280.26349 | 0.9 | 5.11 (5.48) | 0.05 (0.00) | −95.0 | 0.005 | 0.017 |
| *N*-Acetylleucine | 2.920 | $C_8H_{15}NO_3$ | $[M+H]^+$ | 174.11209 | 174.11230 | −1.2 | 2.76 (3.64) | 0.02 (0.00) | −120.3 | 0.005 | 0.017 |
| PC O-18:1 | 12.398 | $C_{26}H_{52}NO_7P$ | $[M+H]^+$ | 522.35602 | 522.35541 | 1.2 | 2.59 (0.86) | 0.02 (0.00) | −133.9 | 0.005 | 0.017 |
| LPC 18:1 | 12.397 | $C_{26}H_{52}NO_7P$ | $[M+Na]^+$ | 544.3385 | 544.33734 | 2.1 | 2.35 (0.56) | 0.02 (0.00) | −151.9 | 0.005 | 0.017 |
| Linoleoylglycine | 8.775 | $C_{20}H_{35}NO_3$ | $[M+Na]^+$ | 320.25613 | 320.25839 | −7.1 | 2.48 (2.77) | 0.01 (0.00) | −153.7 | 0.005 | 0.017 |
| Oleamide | 8.775 | $C_{18}H_{35}NO$ | $[M+H-H_2]^+$ | 280.26425 | 280.26349 | 2.7 | 6.13 (6.71) | 0.02 (0.00) | −253.4 | 0.005 | 0.017 |
| LPC 18:3-SN1 | 9.679 | $C_{26}H_{48}NO_7P$ | $[M+H]^+$ | 518.32361 | 518.32410 | −0.9 | 0.78 (0.22) | 0.00 (0.00) | −262.5 | 0.005 | 0.017 |
| 1-Myristoyl-sn-glycero-3-phosphocholine | 9.571 | $C_{22}H_{46}NO_7P$ | $[M+H]^+$ | 468.30911 | 468.30850 | 1.3 | 0.88 (0.22) | 0.00 (0.00) | −262.8 | 0.005 | 0.017 |
| 1-Oleoyl-sn-glycero-3-phosphocholine | 12.196 | $C_{26}H_{52}NO_7P$ | $[M+H]^+$ | 522.35565 | 522.35541 | 0.5 | 1.50 (0.18) | 0.01 (0.00) | −267.3 | 0.005 | 0.017 |
| Neofusapyrone | 11.065 | $C_{34}H_{54}O_9$ | $[M+H]^+$ | 571.35883 | 571.36292 | −7.2 | 1.19 (0.37) | 0.01 (0.00) | −294.0 | 0.005 | 0.017 |
| LPC 16:0 | 11.556 | $C_{24}H_{50}NO_7P$ | $[M+Na]^+$ | 518.32312 | 518.32172 | 2.7 | 3.45 (2.80) | 0.02 (0.00) | −308.4 | 0.005 | 0.017 |
| LPC 15:0-SN1 | 10.589 | $C_{23}H_{48}NO_7P$ | $[M+H]^+$ | 482.32422 | 482.32413 | 0.2 | 1.14 (0.27) | 0.00 (0.00) | −398.0 | 0.005 | 0.017 |
| PC O-20:5 | 10.232 | $C_{28}H_{48}NO_7P$ | $[M+H]^+$ | 542.32288 | 542.32410 | −2.2 | 2.89 (0.37) | 0.00 (0.00) | −635.1 | 0.005 | 0.017 |

The data represent the median and interquartile range [Q1; Q3] for the basal time point and day 7, with values normalized by dividing by 10,000. The fold change (FC) was calculated as the median of basal values divided by the median of day 7 values. The false discovery rate (FDR) is the adjusted *p*-value obtained from a paired Mann–Whitney test. Retention time ($R_t$) is reported in minutes. AUDA: 12-[[(tricyclo[1,3,7,13]dec-1-ylamino)carbonyl]amino]-dodecanoic acid; Cer: Ceramide; LPC: Lysophosphatidylcholine; PC O: 1-alkyl, 2-acylglycerophosphocholines; SPB: sphingosines; DGGA: diacylglycerols.

The pathway analysis indicated that the metabolites that showed significant differences between baseline and day 7 were those related to glycerophospholipid, caffeine, glycine, serine and threonine, arginine and proline, and linoleic acid metabolism (Figure 7C). These results suggest a reconfiguration of lipid and amino acid metabolism due to CSE supplementation. Additionally, enrichment in xanthines and cholines (key components in neurochemical and membrane dynamics), 6-aminopurines (indicative of nucleotide turnover), and sphingosines (suggestive of changes in lipid signaling molecules) was observed. This indicates broad-spectrum metabolic modulation, affecting both energy and structural molecule pathways. Although less pronounced, amino acids also had a role in the metabolic adaptation observed in this study (Figure 7D).

Overall, the results demonstrate significant metabolic reconfiguration induced by CSE supplementation, affecting multiple pathways related to lipid metabolism, amino acid turnover, and energy homeostasis.

### *3.4. Network Analysis Elucidated Metabolic Pathways Altered by CSE Supplementation*

The metabolic analysis conducted highlighted several significant pathways and modules, each contributing to a complex network of biochemical interactions (Figure 8A). The analysis of metabolic pathways revealed notable changes in the cholinergic synapse ($p = 1.0 \times 10^{-6}$) and glycerophospholipid metabolism ($p = 2.1 \times 10^{-5}$), crucial for maintaining cellular communication, maintaining neurotransmission, and influencing cognitive functions and muscle control (Figure 8B). The retrograde endocannabinoid signaling ($p = 3.5 \times 10^{-6}$) and glutamatergic synapse pathway ($p = 1.5 \times 10^{-5}$) indicate significant changes in neurotransmission processes. Endocannabinoid signaling modulates various physiological processes, including pain sensation, mood, appetite, and memory, while the glutamatergic synapse pathway is involved in excitatory neurotransmission, crucial for synaptic plasticity and cognitive functions. The phospholipase D signaling pathway ($p = 1.9 \times 10^{-3}$) also showed significant alterations, underscoring disruptions in lipid signaling processes, which are critical in cell growth, differentiation, and immune responses, as they generate phosphatidic acid. Additionally, the nucleotide metabolism pathway ($p = 1.0 \times 10^{-3}$) and caffeine metabolism pathway ($p = 2.8 \times 10^{-3}$) reflect energy and purine metabolism shifts, respectively. In terms of metabolic modules, the creatine pathway ($p = 1.0 \times 10^{-6}$) and betaine biosynthesis pathway ($p = 1.0 \times 10^{-6}$) are crucial for cellular energy storage and methylation reactions, which are vital for energy production in muscle and brain tissues (Figure 8B). Betaine biosynthesis is important for the methylation of homocysteine to methionine. The methionine salvage pathway ($p = 4.1 \times 10^{-3}$) and phosphatidylcholine biosynthesis ($p = 5.9 \times 10^{-5}$) highlight the importance of sulfur amino acid metabolism and phospholipid synthesis. The phosphatidylethanolamine biosynthesis via ethanolamine ($p = 3.2 \times 10^{-4}$) and phosphatidylethanolamine biosynthesis via phosphatidylserine decarboxylase ($p = 4.6 \times 10^{-3}$) emphasize significant lipid metabolic shifts. Finally, the purine degradation pathway ($p = 3.8 \times 10^{-3}$) and adenine ribonucleotide degradation pathway ($p = 1.0 \times 10^{-6}$) suggest alterations in nucleotide turnover, critical for cellular proliferation and energy metabolism, which are essential for maintaining nucleotide balance and energy homeostasis. The guanine ribonucleotide degradation pathway ($p = 1.0 \times 10^{-6}$) and polyamine biosynthesis ($p = 1.8 \times 10^{-5}$) indicate changes in cell growth and differentiation processes.

Overall, the integrated analysis of pathways and modules highlights a broad spectrum of metabolic alterations. These findings underscore the complexity of metabolic regulation and the significant impact of metabolic changes on cellular and systemic functions. This analysis brings forward key insights into the altered biochemical landscape, paving the way for a deeper understanding of metabolic diseases and potential intervention points. The observed changes in the plasma metabolome suggest that CSE has the potential to influence key physiological processes, supporting its use as a nutraceutical with diverse health benefits.

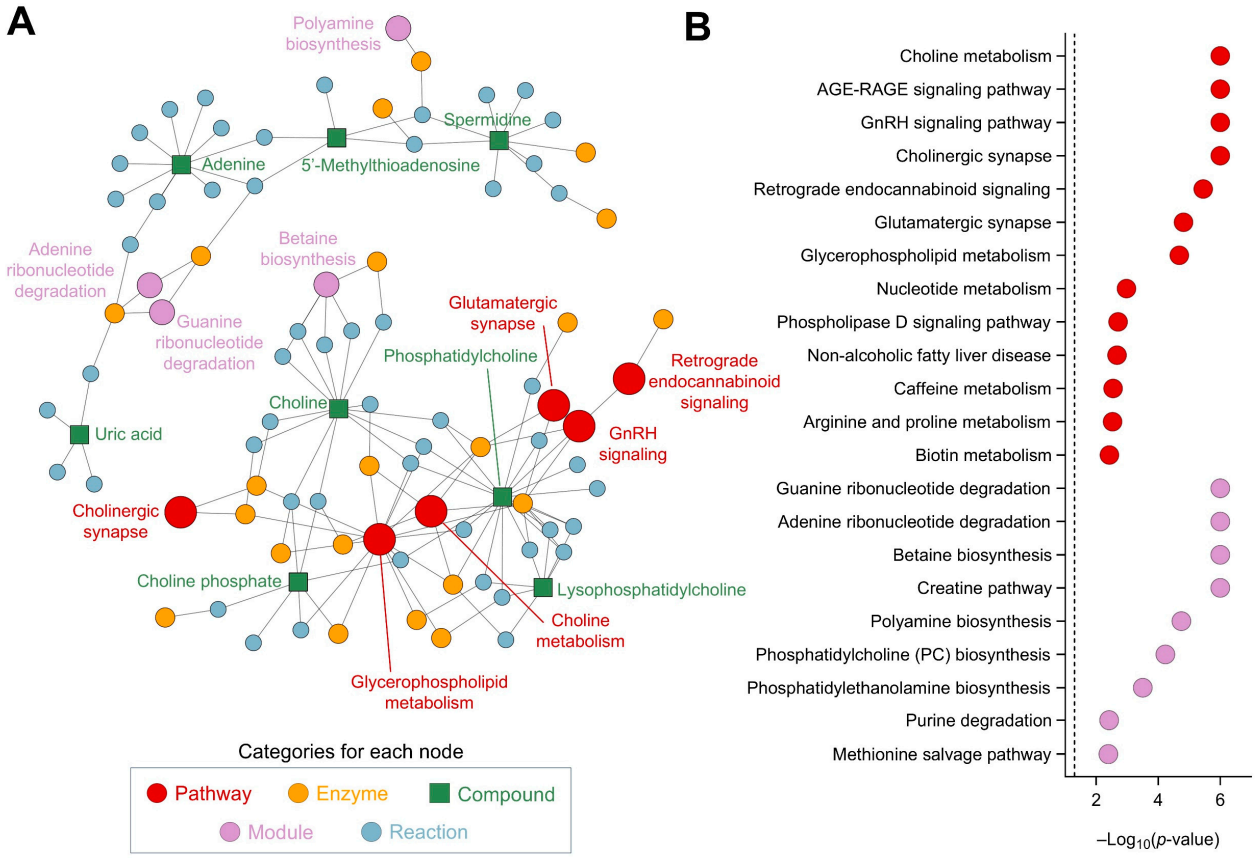


**Figure 8.** Network and pathway analysis, using FELLA, of the metabolites affected by CSE supplementation, including a network representation of the metabolic pathways, modules, enzymes, and reactions impacted by CSE supplementation (**A**), and a dot plot of the significantly affected pathways and modules, showing their −log10(*p*-value) scores (**B**). Nodes represent different categories: pathways (red, ●), enzymes (yellow, ●), compounds (green, ■), modules (purple, ●), and reactions (blue, ●). The size of the nodes corresponds to the significance of their involvement, with larger nodes indicating higher relevance.

## 4. Discussion

The present study evaluates the metabolic changes induced by CSE supplementation in rats for the first time. Our findings reveal significant modifications in metabolites associated with glycerophospholipid metabolism, amino acid processing, and methylxanthine bioavailability, indicating a multifaceted effect of the CSE on physiological pathways. The distinctive clusters observed for baseline, day 4, and day 7 not only demonstrate the time-dependent metabolic changes caused by CSE, but also highlight the speed with which these changes occurred. Interestingly, as early as day 7, the plasma metabolome had undergone considerable reconfiguration, indicating the significant metabolic effect of a CSE supplementation. Secondly, by analyzing methylxanthines' bioavailability in rat plasma, we were able to provide insight into CSE's caffeine and theobromine metabolic rate. The presence of caffeine and theobromine in rats' plasma confirms the effective absorption and systemic distribution of these methylxanthines after CSE administration. Our analysis identified significant alterations in several key pathways: the cholinergic synapse, glycerophospholipid metabolism, retrograde endocannabinoid signaling, glutamatergic synapse, and phospholipase D signaling. These pathways are vital for cellular communication, neurotransmission, cognitive functions, and muscle control. The observed changes suggest disruptions in lipid signaling, which is crucial for processes such as cell growth and differentiation, immune responses, energy and purine metabolism, membrane structure,

protein synthesis, and inflammation regulation. These metabolic changes underline the broad-spectrum influence of CSE on metabolism homeostasis.

Our results indicate that the metabolic profile was not markedly different between the basal time point and day 4 of supplementation, suggesting that a short period of CSE supplementation may not be sufficient to induce marked changes in metabolic pathways. Nonetheless, we observed that caffeine metabolism was detectable in the rat plasma on day 4, demonstrating the bioavailability of methylxanthines (caffeine and theobromine) present in CSE. The presence of caffeine may explain the antioxidant properties and vasodilatation that we have previously shown in vascular tissue with CSE or caffeine supplementation [5]. Caffeine's mechanism for enhancing vasodilation likely involves inhibiting phosphodiesterase, leading to an increase in cAMP within vascular smooth muscle cells, which promotes relaxation. Additionally, the antioxidant effects of caffeine may derive from its capability to modulate signaling pathways that activate endogenous antioxidant defenses [22]. The presence of caffeine may also contribute to the blood pressure-lowering effects of 2-week CSE supplementation in vivo by upregulating endothelial nitric oxide synthase (e-NOS) and the antioxidant response element nuclear factor (erythroid-derived 2)-like 2 (Nrf2) [16]. It has traditionally been considered that caffeine should be approached with caution in the context of hypertension; however, recent epidemiological data indicate that moderate and habitual consumption of caffeinated coffee does not adversely affect blood pressure and protects against cardiovascular diseases [23,24], which is in agreement with the blood-pressure-lowering effects of CSE supplementation observed in rats.

An increase in glycerophospholipid metabolism was one of the relevant metabolic modifications observed after CSE supplementation, likely reflecting changes in membrane fluidity and signaling that are critical for cardiovascular health and cognitive function. Particularly, the decrease in PC O-20:5 and DHA methyl ester suggests increased utilization of omega-3 fatty acids, altering lipid-mediated signaling and inflammation. These fatty acids, incorporated in cell membranes, are substrates for specialized pro-resolving mediators (SPMs), which inhibit platelets, release NO, and reduce inflammation [25,26]. Omega-3 fatty acids are also essential for neuronal function and cognitive health, contributing to synaptic plasticity and neurotransmission [27,28]. The increase in phosphatidylcholine biosynthesis supports the synthesis of acetylcholine, a key neurotransmitter involved in learning and memory, and has been linked to improved cognitive function [29]. Furthermore, the increase in lysophosphatidylcholines, such as LPC O-13:1, points to dynamic changes in cell membrane compositions that might enhance endothelial function and contribute to improved vascular responses. Plasma lysophosphatidylcholines are negatively correlated with inflammatory markers in patients with myocardial infarction [30], and are also decreased in atherosclerosis and vascular damage [31]. In addition, lysophosphatidylcholines have been shown to influence cognitive function and neurotransmission by acting on G-protein-coupled receptors and modulating synaptic activity, thereby promoting neuronal health [32,33]. The abovementioned metabolic shifts could directly contribute to the observed improvements in cardiovascular function and cognitive health, thereby supporting the potential benefits of CSE supplementation.

Other metabolomic studies evidence that supplementation with polyphenol-rich plants exerts important modifications in glycerophospholipid metabolism, improving obesity-related alterations [34,35]. The changes in sphingolipid metabolism, particularly ceramide levels, indicate a significant impact of CSE on cellular signaling. Ceramides regulate cell membranes, apoptosis, and signal transduction [36]. Their modulation by CSE may enhance cellular resilience to oxidative stress, mitigating inflammation and reducing oxidative damage, as shown in our previous studies in vitro in cell culture models and ex

vivo in arteries [4,5]. These effects are particularly relevant in the context of inflammation and oxidative stress illnesses, such as cardiovascular diseases and metabolic disorders, contributing to reducing blood pressure in aged hypertensive animals [16].

The observed decrease in plasmatic amino acids, such as tyrosine and creatine, marks a significant adaptation in nitrogen balance and energy metabolism following CSE supplementation. Reducing tyrosine, a precursor to neurotransmitters like dopamine and norepinephrine, could suggest alterations in catecholamine metabolism [37,38]. Additionally, CSE's modulation of choline metabolism suggests impacts on neural processes and muscle function. As a key component in acetylcholine synthesis, essential for brain and muscle function, enhanced choline turnover could imply improved cognitive and neural communication due to CSE's bioactive compounds [39]. Moreover, the decrease in creatine, which is crucial for energy storage and transfer, suggests a shift in energy management strategies. Reduced creatine could indicate increased fatty acid oxidation or enhanced glucose metabolism, enhancing metabolic flexibility [40,41]. Hence, these adjustments, influenced by CSE's bioactive compounds, may optimize energy usage and neurotransmitter balance to enable individuals to better cope with physiological stressors.

Furthermore, decreased glutathione metabolism post-CSE supplementation may indicate reduced oxidative stress due to CSE's antioxidant properties. While increased glutathione is typically linked to enhanced antioxidant defense, a decrease might suggest that CSE's (poly)phenols or methylxanthines mitigate oxidative challenges, reducing reliance on glutathione. This reflects an adaptive optimization of the cellular antioxidant system. CSE intake has also been shown to improve the Nrf2 pathway in cardiovascular tissue and increase GSH in plasma from aged hypertensive rats [16]. The changes in nicotinate and nicotinamide metabolism impact cellular health. Nicotinamide adenine dinucleotide ($NAD^+$), a product of this pathway, is vital for energy production and serves as a substrate for DNA repair enzymes [42]. Simultaneously, alterations in 6-aminopurine metabolism, particularly adenine, highlight an effect on purine metabolism. These alterations suggest that CSE supplementation enhances cellular repair and regeneration, helping to maintain cellular integrity under metabolic stress [43]. Additionally, CSE is rich in (poly)phenols with antioxidant and anti-inflammatory properties. Although not directly detected in rat plasma due to the analytical methods employed, their biochemical influence likely contributed to observed metabolic changes. Cocoa shell (poly)phenols can enhance antioxidant defenses, modulate endogenous systems like glutathione [44], regulate gene expression related to metabolism and inflammation [4], and influence lipid and energy metabolism pathways [45].

This research offers noteworthy preliminary findings on the impact of cocoa shell intake on the plasma metabolome in rats. However, there are significant limitations to consider. Firstly, metabolic responses can differ between species, which might lead to inconsistencies when extrapolating results from rats to humans. Secondly, the analysis was primarily focused on plasma metabolome changes, which may ignore potential impacts on other tissues or fluids. Thirdly, the study was conducted exclusively in female rats over a short-term period (7 days), limiting conclusions regarding potential sex-dependent differences or long-term metabolic effects. Future studies should assess male subjects and extended supplementation durations to evaluate these factors. Fourthly, the study used an untargeted metabolomics approach, which, despite allowing an unbiased exploration of the metabolome, might fail to detect certain metabolites that exist in low concentrations or are better suited to a targeted investigation. Additionally, the study only used LC-QTOF analysis in the ESI positive mode, possibly missing data obtainable from other modes or analytical techniques. Considering these limitations and initial results, several ideas for future research emerge. Human-based studies are especially important for expanding

our understanding of cocoa shell metabolism and determining its practical health implications. Furthermore, studies should investigate the effects of cocoa shell intake on other physiological systems, such as the gut microbiome, given its role in metabolizing dietary compounds and its influence on overall health. Future research would benefit from using a targeted metabolomics approach for a more precise investigation of specific pathways or molecules of interest altered by the consumption of cocoa shell. Further studies should include longitudinal trials to examine any long-term effects of cocoa shell intake.

Our study provides preliminary insights into the metabolic effects of CSE supplementation, demonstrating significant changes in the plasma metabolome after a 7-day intervention. These changes, mainly affecting glycerophospholipid, amino acid, and fatty acid metabolism, might indicate potential anti-inflammatory and antioxidant activity. The presence of methylxanthines like caffeine and theobromine suggests their contribution to these effects, aligning with their effects on blood pressure regulation, cardiovascular protection, and cognitive function. Thus, our findings support the hypothesis that CSE intake induces metabolic reconfiguration with possible health benefits, offering novel insights into its potential as a bioactive food ingredient or nutraceutical.

## 5. Conclusions

This study demonstrated that CSE supplementation influenced the plasma metabolome of female rats, specifically via modulating lipid metabolism, amino acid pathways, and methylxanthine bioavailability. The metabolic alterations indicate potential functional properties of CSE; however, due to species-specific differences, any extrapolation to humans must be undertaken with caution. Future research should investigate long-term supplementation and sex-specific metabolic differences, as well as conducting targeted mechanistic studies in human subjects to assess the wider effects of CSE consumption. Our findings emphasize the practical implications of including CSE, a sustainable cocoa by-product, in dietary interventions targeted at improving metabolic health. This study not only provides new insights into the biological activity of the CSE, but also demonstrates the application of food by-products in promoting health and sustainability.

**Supplementary Materials:** The following supporting information can be downloaded at https://www.mdpi.com/article/10.3390/nu17050885/s1, Supplementary Table S1. Metabolites identified in cocoa shell extract, their associated metabolic pathways, and potential health effects. Supplementary Table S2. Key metabolites detected in rat plasma after cocoa shell extract supplementation, their associated metabolic pathways, and potential health effects.

**Author Contributions:** Conceptualization, M.R.-H., S.M.A. and M.A.M.-C.; methodology, D.R.-C. and M.R.-H.; validation, D.R.-C., M.R.-H. and P.R.-R.; formal analysis, D.R.-C., M.R.-H. and P.R.-R.; investigation, D.R.-C., M.R.-H. and P.R.-R.; resources, S.M.A. and M.A.M.-C.; data curation, D.R.-C.; writing—original draft preparation, D.R.-C. and M.R.-H.; writing—review and editing, M.R.-H., S.R., S.M.A. and M.A.M.-C.; visualization, D.R.-C. and M.R.-H.; supervision, S.M.A. and M.A.M.-C.; project administration, S.M.A. and M.A.M.-C. All authors have read and agreed to the published version of the manuscript.

**Funding:** This research was funded by the COCARDIOLAC project from the Spanish Ministry of Science and Innovation (RTI 2018–097504–B–I00) and the Excellence Line for University Teaching Staff within the Multiannual Agreement between the Community of Madrid and the UAM (2019–2023). M. Rebollo-Hernanz received funding from the program of the Ministry of Universities for the requalification of the Spanish university system (CA1/RSUE/2021–00656).

**Institutional Review Board Statement:** The animal study protocol was approved by the Ethics Review Board of Universidad Autónoma de Madrid and the Regional Committee of Comunidad Autónoma de Madrid (PROEX 19/04; approval date: 20 March 2019).

**Informed Consent Statement:** Not applicable.

**Data Availability Statement:** The original contributions presented in the study are included in the article; further inquiries can be directed to the corresponding authors.

**Conflicts of Interest:** The authors declare no conflicts of interest.

## References


1. Nirmal, N.P.; Khanashyam, A.C.; Mundanat, A.S.; Shah, K.; Babu, K.S.; Thorakkattu, P.; Al-Asmari, F.; Pandiselvam, R. Valorization of Fruit Waste for Bioactive Compounds and Their Applications in the Food Industry. *Foods* **2023**, *12*, 556. [CrossRef] [PubMed]
2. Kumar, K.; Yadav, A.N.; Kumar, V.; Vyas, P.; Dhaliwal, H.S. Food Waste: A Potential Bioresource for Extraction of Nutraceuticals and Bioactive Compounds. *Bioresour. Bioprocess.* **2017**, *4*, 18. [CrossRef]
3. Gil-Ramírez, A.; Cañas, S.; Cobeta, I.M.; Rebollo-Hernanz, M.; Rodríguez-Rodríguez, P.; Benítez, V.; Arribas, S.M.; Martín-Cabrejas, M.A.; Aguilera, Y. Uncovering Cocoa Shell as a Safe Bioactive Food Ingredient: Nutritional and Toxicological Breakthroughs. *Futur. Foods* **2024**, *10*, 100461. [CrossRef]
4. Rebollo-Hernanz, M.; Aguilera, Y.; Martin-Cabrejas, M.A.; Gonzalez de Mejia, E. Phytochemicals from the Cocoa Shell Modulate Mitochondrial Function, Lipid and Glucose Metabolism in Hepatocytes via Activation of FGF21/ERK, AKT, and MTOR Pathways. *Antioxidants* **2022**, *11*, 136. [CrossRef]
5. Rodríguez-Rodríguez, P.; Ragusky, K.; Phuthong, S.; Ruvira, S.; Ramiro-Cortijo, D.; Cañas, S.; Rebollo-Hernanz, M.; Morales, M.D.; López de Pablo, Á.L.; Martín-Cabrejas, M.A.; et al. Vasoactive Properties of a Cocoa Shell Extract: Mechanism of Action and Effect on Endothelial Dysfunction in Aged Rats. *Antioxidants* **2022**, *11*, 429. [CrossRef]
6. Sánchez, M.; Laca, A.; Laca, A.; Díaz, M. Cocoa Bean Shell: A By-Product with High Potential for Nutritional and Biotechnological Applications. *Antioxidants* **2023**, *12*, 1028. [CrossRef]
7. Rojo-Poveda, O.; Barbosa-Pereira, L.; Zeppa, G.; Stévigny, C. Cocoa Bean Shell—A By-Product with Nutritional Properties and Biofunctional Potential. *Nutrients* **2020**, *12*, 1123. [CrossRef]
8. Rebollo-Hernanz, M.; Cañas, S.; Braojos, C.; Cano-Muñoz, P.; Martín-Cabrejas, M.A. Cocoa Shell: Source of Novel Bioactive Ingredients for the Prevention of Cardiometabolic Diseases. In *Molecular Mechanisms of Functional Food*; Campos-Vega, R., Oomah, B.D., Eds.; Wiley: Hoboken, NJ, USA, 2022; pp. 485–519, ISBN 9781119804055.
9. Mozaffarian, D. Dietary and Policy Priorities to Reduce the Global Crises of Obesity and Diabetes. *Nat. Food* **2020**, *1*, 38–50. [CrossRef]
10. Cañas, S.; Rebollo-Hernanz, M.; Braojos, C.; Benítez, V.; Ferreras-Charro, R.; Dueñas, M.; Aguilera, Y.; Martín-Cabrejas, M.A. Gastrointestinal Fate of Phenolic Compounds and Amino Derivatives from the Cocoa Shell: An in Vitro and in Silico Approach. *Food Res. Int.* **2022**, *162*, 112117. [CrossRef]
11. Muthubharathi, B.C.; Gowripriya, T.; Balamurugan, K. Metabolomics: Small Molecules that Matter More. *Mol. Omi.* **2021**, *17*, 210–229. [CrossRef]
12. Guasch-Ferre, M.; Bhupathiraju, S.N.; Hu, F.B. Use of Metabolomics in Improving Assessment of Dietary Intake. *Clin. Chem.* **2018**, *64*, 82–98. [CrossRef] [PubMed]
13. Rafiq, T.; Azab, S.M.; Teo, K.K.; Thabane, L.; Anand, S.S.; Morrison, K.M.; De Souza, R.J.; Britz-Mckibbin, P. Nutritional Metabolomics and the Classification of Dietary Biomarker Candidates: A Critical Review. *Adv. Nutr.* **2021**, *12*, 2333–2357. [CrossRef] [PubMed]
14. Clarke, E.D.; Ferguson, J.; Collins, C.E. Dietary Assessment and Metabolomic Methodologies in Feeding Studies: A Scoping Review. *Proc. Nutr. Soc.* **2023**, *82*, E185. [CrossRef]
15. Rebollo-Hernanz, M.; Cañas, S.; Taladrid, D.; Segovia, Á.; Bartolomé, B.; Aguilera, Y.; Martín-Cabrejas, M.A. Extraction of Phenolic Compounds from Cocoa Shell: Modeling Using Response Surface Methodology and Artificial Neural Networks. *Sep. Purif. Technol.* **2021**, *270*, 118779. [CrossRef]
16. Ruvira, S.; Rodríguez-Rodríguez, P.; Ramiro-Cortijo, D.; Martín-Trueba, M.; Martín-Cabrejas, M.A.; Arribas, S.M. Cocoa Shell Extract Reduces Blood Pressure in Aged Hypertensive Rats via the Cardiovascular Upregulation of Endothelial Nitric Oxide Synthase and Nuclear Factor (Erythroid-Derived 2)-like 2 Protein Expression. *Antioxidants* **2023**, *12*, 1698. [CrossRef]
17. Chen, Y.; Li, E.M.; Xu, L.Y. Guide to Metabolomics Analysis: A Bioinformatics Workflow. *Metabolites* **2022**, *12*, 357. [CrossRef]
18. Tiffany, C.R.; Bäumler, A.J. Omu, a Metabolomics Count Data Analysis Tool for Intuitive Figures and Convenient Metadata Collection. *Microbiol. Resour. Announc.* **2019**, *8*, e00129-19. [CrossRef]
19. Lê, S.; Josse, J.; Husson, F. FactoMineR: An R Package for Multivariate Analysis. *J. Stat. Softw.* **2008**, *25*, 1–18. [CrossRef]
20. Wohlgemuth, G.; Haldiya, P.K.; Willighagen, E.; Kind, T.; Fiehn, O. The Chemical Translation Service-a Web-Based Tool to Improve Standardization of Metabolomic Reports. *Bioinformatics* **2010**, *26*, 2647–2648. [CrossRef]

21. Picart-Armada, S.; Fernández-Albert, F.; Vinaixa, M.; Yanes, O.; Perera-Lluna, A. FELLA: An R Package to Enrich Metabolomics Data. *BMC Bioinform.* **2018**, *19*, 538. [CrossRef]
22. Higashi, Y. Coffee and Endothelial Function: A Coffee Paradox? *Nutrients* **2019**, *11*, 2104. [CrossRef] [PubMed]
23. Rodríguez-Artalejo, F.; López-García, E. Coffee Consumption and Cardiovascular Disease: A Condensed Review of Epidemiological Evidence and Mechanisms. *J. Agric. Food Chem.* **2018**, *66*, 5257–5263. [CrossRef] [PubMed]
24. Borghi, C. Coffee and Blood Pressure: Exciting News! *Blood Press.* **2022**, *31*, 284–287. [CrossRef] [PubMed]
25. So, J.; Wu, D.; Lichtenstein, A.H.; Tai, A.K.; Matthan, N.R.; Maddipati, K.R.; Lamon-Fava, S. EPA and DHA Differentially Modulate Monocyte Inflammatory Response in Subjects with Chronic Inflammation in Part via Plasma Specialized Pro-Resolving Lipid Mediators: A Randomized, Double-Blind, Crossover Study. *Atherosclerosis* **2021**, *316*, 90–98. [CrossRef]
26. Sherratt, S.C.R.; Libby, P.; Budoff, M.J.; Bhatt, D.L.; Mason, R.P. Role of Omega-3 Fatty Acids in Cardiovascular Disease: The Debate Continues. *Curr. Atheroscler. Rep.* **2023**, *25*, 1–17. [CrossRef]
27. Rao, A.S.; Nair, A.; Nivetha, K.; Ayesha, B.; Hardi, K.; Divya, V.; Veena, S.M.; Anantharaju, K.S.; More, S.S. Impacts of Omega-3 Fatty Acids, Natural Elixirs for Neuronal Health, on Brain Development and Functions. *Methods Mol. Biol.* **2024**, *2761*, 209–229. [CrossRef]
28. Hachem, M.; Nacir, H. Emerging Role of Phospholipids and Lysophospholipids for Improving Brain Docosahexaenoic Acid as Potential Preventive and Therapeutic Strategies for Neurological Diseases. *Int. J. Mol. Sci.* **2022**, *23*, 3969. [CrossRef]
29. Roy, P.; Tomassoni, D.; Nittari, G.; Traini, E.; Amenta, F. Effects of Choline Containing Phospholipids on the Neurovascular Unit: A Review. *Front. Cell. Neurosci.* **2022**, *16*, 988759. [CrossRef]
30. Xia, J.G.; Li, B.; Zhang, H.; Li, Q.X.; Lam, S.M.; Yin, C.L.; Tian, H.; Shui, G. Precise Metabolomics Defines Systemic Metabolic Dysregulation Distinct to Acute Myocardial Infarction Associated with Diabetes. *Arterioscler. Thromb. Vasc. Biol.* **2023**, *43*, 581–596. [CrossRef]
31. Paapstel, K.; Kals, J.; Eha, J.; Tootsi, K.; Ottas, A.; Piir, A.; Jakobson, M.; Lieberg, J.; Zilmer, M. Inverse Relations of Serum Phosphatidylcholines and Lysophosphatidylcholines with Vascular Damage and Heart Rate in Patients with Atherosclerosis. *Nutr. Metab. Cardiovasc. Dis.* **2018**, *28*, 44–52. [CrossRef]
32. Geraldo, L.H.M.; Spohr, T.C.L.d.S.; Amaral, R.F.d.; Fonseca, A.C.C.d.; Garcia, C.; Mendes, F.d.A.; Freitas, C.; dosSantos, M.F.; Lima, F.R.S. Role of Lysophosphatidic Acid and Its Receptors in Health and Disease: Novel Therapeutic Strategies. *Signal Transduct. Target. Ther.* **2021**, *6*, 45. [CrossRef]
33. Hao, Y.; Guo, M.; Feng, Y.; Dong, Q.; Cui, M. Lysophospholipids and Their G-Coupled Protein Signaling in Alzheimer's Disease: From Physiological Performance to Pathological Impairment. *Front. Mol. Neurosci.* **2020**, *13*, 529384. [CrossRef] [PubMed]
34. Zhu, Y.; Wei, Y.L.; Karras, I.; Cai, P.J.; Xiao, Y.H.; Jia, C.L.; Qian, X.L.; Zhu, S.Y.; Zheng, L.J.; Hu, X.; et al. Modulation of the Gut Microbiota and Lipidomic Profiles by Black Chokeberry (*Aronia Melanocarpa* L.) Polyphenols via the Glycerophospholipid Metabolism Signaling Pathway. *Front. Nutr.* **2022**, *9*, 913729. [CrossRef] [PubMed]
35. Shen, J.; Li, X.; Zhang, X.; Li, Z.; Abulaiti, G.; Liu, Y.; Yao, J.; Zhang, P. Effects of Xinjiang Wild Cherry Plum (Prunus Divaricata Ledeb) Anthocyanin-Rich Extract on the Plasma Metabolome of Atherosclerotic ApoE-Deficient Mice Fed a High-Fat Diet. *Front. Nutr.* **2022**, *9*, 923699. [CrossRef] [PubMed]
36. Gaggini, M.; Ndreu, R.; Michelucci, E.; Rocchiccioli, S.; Vassalle, C. Ceramides as Mediators of Oxidative Stress and Inflammation in Cardiometabolic Disease. *Int. J. Mol. Sci.* **2022**, *23*, 2719. [CrossRef]
37. Mayorga-Gross, A.L.; Esquivel, P. Impact of Cocoa Products Intake on Plasma and Urine Metabolites: A Review of Targeted and Non-Targeted Studies in Humans. *Nutrients* **2019**, *11*, 1163. [CrossRef]
38. Ryan, P.J.; Riechman, S.E.; Fluckey, J.D.; Wu, G. Interorgan Metabolism of Amino Acids in Human Health and Disease. *Adv. Exp. Med. Biol.* **2021**, *1332*, 129–149. [CrossRef]
39. Vyas, C.M.; Manson, J.A.E.; Sesso, H.D.; Rist, P.M.; Weinberg, A.; Kim, E.; Moorthy, M.V.; Cook, N.R.; Okereke, O.I. Effect of Cocoa Extract Supplementation on Cognitive Function: Results from the Clinic Subcohort of the COSMOS Trial. *Am. J. Clin. Nutr.* **2024**, *119*, 39–48. [CrossRef]
40. Guerra, I.M.S.; Ferreira, H.B.; Melo, T.; Rocha, H.; Moreira, S.; Diogo, L.; Domingues, M.R.; Moreira, A.S.P. Mitochondrial Fatty Acid β-Oxidation Disorders: From Disease to Lipidomic Studies—A Critical Review. *Int. J. Mol. Sci.* **2022**, *23*, 13933. [CrossRef]
41. Kazak, L.; Cohen, P. Creatine Metabolism: Energy Homeostasis, Immunity and Cancer Biology. *Nat. Rev. Endocrinol.* **2020**, *16*, 421–436. [CrossRef]
42. Dunwoodie, S.L.; Bozon, K.; Szot, J.O.; Cuny, H. Nicotinamide Adenine Dinucleotide Deficiency and Its Impact on Mammalian Development. *Antioxid. Redox Signal.* **2023**, *39*, 1108–1132. [CrossRef] [PubMed]
43. Huang, Z.; Xie, N.; Illes, P.; Di Virgilio, F.; Ulrich, H.; Semyanov, A.; Verkhratsky, A.; Sperlagh, B.; Yu, S.G.; Huang, C.; et al. From Purines to Purinergic Signalling: Molecular Functions and Human Diseases. *Signal Transduct. Target. Ther.* **2021**, *6*, 162. [CrossRef] [PubMed]

44. Cañas, S.; Rebollo-Hernanz, M.; Bermúdez-Gómez, P.; Rodríguez-Rodríguez, P.; Braojos, C.; Gil-Ramírez, A.; Benítez, V.; Aguilera, Y.; Martín-Cabrejas, M.A. Radical Scavenging and Cellular Antioxidant Activity of the Cocoa Shell Phenolic Compounds after Simulated Digestion. *Antioxidants* **2023**, *12*, 1007. [CrossRef] [PubMed]
45. Braojos, C.; Rebollo-Hernanz, M.; Cañas, S.; Aguilera, Y.; Gil-Ramírez, A.; Benítez, V.; Martín-Cabrejas, M.A. Cocoa Shell Ingredients Improve Their Lipid-Lowering Properties under Simulated Digestion: In Vitro and HepG2 Cells Study. *Food Res. Int.* **2024**, *196*, 115037. [CrossRef]